Structural Properties and Deformation Patterns of Evolving Strike-slip Faults: Numerical Simulations Incorporating Damage Rheology

Yaron Finzi,[1] Elizabeth H. Hearn,[1] Yehuda Ben-Zion,[2] and Vladimir Lyakhovsky[3]

Abstract—We present results on evolving geometrical and material properties of large strike-slip fault zones and associated deformation fields, using 3-D numerical simulations in a rheologically-layered model with a seismogenic upper crust governed by a continuum brittle damage framework over a viscoelastic substrate. The damage healing parameters we employ are constrained using results of test models and geophysical observations of healing along active faults. The model simulations exhibit several results that are likely to have general applicability. The fault zones form initially as complex segmented structures and evolve overall with continuing deformation toward contiguous, simpler structures. Along relatively-straight mature segments, the models produce flower structures with depth consisting of a broad damage zone in the top few kilometers of the crust and highly localized damage at depth. The flower structures form during an early evolutionary stage of the fault system (before a total offset of about 0.05 to 0.1 km has accumulated), and persist as continued deformation localizes further along narrow slip zones. The tectonic strain at seismogenic depths is concentrated along the highly damaged cores of the main fault zones, although at shallow depths a small portion of the strain is accommodated over a broader region. This broader domain corresponds to shallow damage (or compliant) zones which have been identified in several seismic and geodetic studies of active faults. The models produce releasing stepovers between fault zone segments that are locations of ongoing interseismic deformation. Material within the fault stepovers remains damaged during the entire earthquake cycle (with significantly reduced rigidity and shear-wave velocity) to depths of 10 to 15 km. These persistent damage zones should be detectable by geophysical imaging studies and could have important implications for earthquake dynamics and seismic hazard.

Key words: Damage rheology, fault zone structure, strike-slip fault evolution, compliant zones, fault stepovers.

1. Introduction

Understanding the geometrical and mechanical properties of fault zones is important for many geoscience fields, including earthquake mechanics, crustal hydrology and mineral exploration. Since crustal faults generally grow and evolve through repeated earthquake ruptures, there are fundamental feedback mechanisms between the earth-

[1] Department of Earth and Ocean Sciences, University of British Columbia, Vancouver B.C. V6T 1Z4, Canada. E-mail: yfinzi@eos.ubc.ca; ehearn@eos.ubc.ca

[2] Department of Earth Sciences, University of Southern California Los Angeles, CA 90089-0740, U.S.A. E-mail: benzion@usc.edu

[3] Geological Survey of Israel, Jerusalem 95501, Israel. E-mail: vladi@geos.gsi.gov.il

quakes sustained by a fault and its structural evolution. Observational and theoretical studies indicate that the temporal and frequency-size statistics of earthquakes change as faults evolve with cumulative slip, from disordered structures to more regular mature fault zones (e.g., WESNOUSKY, 1994; BEN-ZION, 1996; STIRLING *et al.*, 1996; LYAKHOVSKY *et al.*, 2001). The evolution of the permeability structures around large faults affects the fluid flow properties of the crust and deposition of minerals (e.g., MICKLETHWAITE and COX, 2004). The evolving fluid flow regime influences in turn the mechanics of earthquakes and faults (e.g., HICKMAN *et al.*, 1995 and references therein). Fault stepovers and other geometrical heterogeneities affect the initiation, propagation and termination of earthquakes (e.g., SIBSON, 1985; KING, 1986; HARRIS and DAY, 1999; OGLESBY *et al.*, 2003; WESNOUSKY, 2006). Contrasts of elastic and permeability properties across faults affect the mode and properties of dynamic ruptures, seismic radiation and aseismic slip (e.g., BEN-ZION and ANDREWS, 1998; RUDNICKI and RICE, 2006; YAMASHITA, 2007; AMPUERO and BEN-ZION, 2008; DUNHAM and RICE, 2008).

Detailed mapping of several exhumed fault zones (e.g., CHESTER *et al.*, 1993; EVANS *et al.*, 2000; SIBSON, 2003) and additional observations summarized by BEN-ZION and SAMMIS (2003) indicate that the internal structure of fault zones evolves from an early stage associated with distributed deformation and band-limited fractal structures at several hierarchies, through localization to principal slip zones, to a mature stage characterized by large-scale faults with tabular damage zones and narrow cores of ultra-cataclasites. However, the ranges of conditions over which such evolution takes place, and the coupling between the evolving structures and distributions of crustal stress and strain, are not well understood. Various studies attempted to model changes of fault properties with ongoing deformation. For example, OLSON and POLLARD (1989) modeled the evolution of joints based on linear elastic fracture mechanics. COWIE *et al.* (1993) simulated evolving geometrical properties of fault networks using a scalar elastic field on a lattice model with spring-like elements. ANDREWS (2005), BEN-ZION and SHI (2005) and TEMPLETON and RICE (2008) simulated the generation of off-fault plastic strain during propagation of dynamic ruptures on frictional faults surrounded by a solid governed by Coulomb plastic yielding. While these studies provide important insights for various topics, they do not account for the evolution of elastic properties that accompanies the generation of cracking and inelastic strain, and they are also typically done within 2-D "plane strain" frameworks.

In the present work we attempt to understand some general aspects of the evolution of large strike-slip fault zone structures. The study is based on three-dimensional numerical simulations with a regional lithospheric model consisting of a seismogenic crust governed by damage rheology over a viscoelastic substrate (BEN-ZION and LYAKHOVSKY, 2006). Using this framework with parameters constrained by laboratory and geophysical observations, we examine the evolving geometrical and elastic properties of fault zones and the associated deformation patterns.

In the next section we summarize observational results on fault zone structures that are relevant to our study. In Section 3 we review the damage rheology framework and

key aspects of the numerical model employed in this work. In Section 4 we use geophysical observations of strength degradation and recovery within active fault zones to narrow the range of admissible damage rheology parameters. Section 5 contains the results of our parameter-space study on structural evolution of large strike-slip fault zones. Our simulations produce for ranges of realistic conditions flower structures with depth and secondary faulting within stepovers comparable to those documented in geological and seismic studies. The results support the view that fault zones display highly localized slip embedded within a wider shallow damage zone. The implications of the results to plate boundary dynamics and suggestions for continuing studies are discussed in Section 6.

2. Geological and Geophysical Observations of Fault Zone Structure

The geometrical properties of fault structures and earthquake slip zones have been documented in many geological and geophysical studies. In general, strike-slip fault zones display a nested hierarchy of damage zones and slip surfaces that form "flower structures" with depth (e.g., WILCOX et al., 1973; SYLVESTER and SMITH, 1976; SYLVESTER, 1988). In a typical fault structure, the principal slip zone is surrounded by gouge and embedded within a tabular or wedge-shaped damage zone (BEN-ZION and SAMMIS, 2003, and references therein). The extent of the damage zone may be defined as the region in which the density of deformation features exceeds the average regional level of deformation in the surrounding host rock (CHESTER, 1995).

Studies of earthquake slip in exhumed faults and paleoseismic trenches indicate that within the top few kilometers of the crust the majority of coseismic slip is accommodated along very narrow slip zones (e.g., SIBSON, 2003; ROCKWELL and BEN-ZION, 2007). The highly localized slip zone and surrounding ultracataclasite layer are referred to as the "core" of the fault zone. This fault core is typically parallel to the macroscopic slip vector and is surrounded by a cataclasite layer which is a few meters thick (e.g., CHESTER and CHESTER, 1998; SCHULZ and EVANS, 2000). The damage zone (DZ) around the fault core typically consists of a zone of intense damage, and possibly pulverized rocks, with a width of a few hundred meters (DOR et al., 2006, 2008), which is surrounded by a broader, several kilometers wide zone, of distributed damage. The latter is probably a relic structure of the progressive coalescence and localization of the active fault zone over time (AMBRASEYS, 1970; KIM et al., 2004; SIBSON, 2003).

The near-surface observations of distributed DZ are supported and complemented by a variety of geophysical studies that associate the DZ with a negative gravity anomaly and low seismic velocities (e.g., STIERMAN, 1984; MOONEY and GINZBURG, 1986), along with anisotropic seismic waves (e.g., COCHRAN et al., 2003; LIU et al. 2004; PENG and BEN-ZION, 2004, 2005) and elevated seismic scattering (e.g., REVENAUGH, 2000). Within the fault zone, seismic waves may be trapped in a narrow zone of intense coherent damage that is significantly distinct from the wider distributed damage zone (e.g., BEN-ZION and AKI,

1990; LI *et al., 1990*). Such fault zone trapped waves have been observed along large faults of the North Anatolian Fault System (NAFS), the Eastern California Shear Zone (ECSZ) and the San Andreas Fault System (e.g., LI *et al., 1994*; BEN-ZION *et al., 2003*). Systematic inversions of trapped waves indicate ~ 100 m wide tabular zones that extend typically to ~ 3–4 km depth and are characterized by strong attenuation and ~ 30–50% shear-wave velocity (V_s) reduction relative to their surroundings (PENG *et al., 2003*; KORNEEV *et al., 2003*; LEWIS *et al., 2005*).

Damage zones also show up in geodetic measurements that detect amplification of deformation signals along fault zones. BEN-ZION *et al.* (1990) observed amplified strain and water-level signals at several locations along the Mojave segment of the San Andreas fault. FIALKO *et al.* (2002) and HAMIEL and FIALKO (2007) interpreted measurements of Interferometeric Synthetic Aperture Radar (InSAR) along several large strike-slip faults in terms of compliant zones that are 1–2 kilometers wide, 3 km to over 10 km deep, and which have rigidity (μ) reduction of 50%–70% relative to the host rock. The discrepancies in dimensions (particularly, width) of the geodetically determined "compliant zones" and seismically determined "trapping structures" probably reflect differences between the broader long-term, quasi-passive, damage structure and the narrower active zone associated with recent earthquake ruptures. Other effects may feed into these discrepancies. For example, distributed microfractures affect the geodetically observed static strength more than they affect the seismically observed dynamic strength of rock (e.g., IDE, 1936; EISSA and KAZI, 1988). Other seismic observations such as seismic anisotropy (e.g., COCHRAN *et al.*, 2003; LIU *et al.* 2004; PENG and BEN-ZION, 2004, 2005) and elevated scattering (e.g., REVENAUGH, 2000) near large faults conform with the geodetically determined wide damage zones (1–2 km wide at the top few kilometers), indicating perhaps that the "trapping structures" are much smaller than the entire damage zone.

To date, the best evidence of high localization of seismic slip at depths larger than 3–5 km is associated with the general tendency of seismicity to localize along relatively-straight fault segments to zones with width that is comparable to the smallest dimension that is resolvable by the data analysis. In places with good network coverage and relocated seismicity, the width of such zones is only a few tens of meters (e.g., POUPINET *et al.*, 1984; NADEAU *et al.*, 1994; SCHAFF *et al.*, 2002; MCGUIRE and BEN-ZION, 2005; THURBER *et al.*, 2006).

A significant deviation from the relatively simple DZ structure described above occurs at fault stepover zones. Fault zones generally display higher geometrical complexity and broader damage zones within stepovers than along relatively straight segments. While the major fault segments reflect a positive feedback of strain weakening and strain localization along the fault cores, persisting geometrical features such as fault offsets, kinks, and bends, can produce strain hardening that leads to local complexity and secondary fractures at different scales (BEN-ZION and SAMMIS, 2003). Many studies have characterized macroscopic structural features within enlarged damage zones at geometrical irregularities (e.g., SEGALL and POLLARD, 1980; KIM *et al.,* 2004). Our study attempts

to clarify the evolution of structural properties of fault zones along relatively straight segments as well as near large persisting stepovers.

3. Damage Rheology Framework

3.1. Theoretical Background

In the past decade continuum damage mechanics models have been successfully applied (e.g., BERCOVICI and RICARD, 2003; TURCOTTE and GLASSCOE, 2004) in various studies of long-term tectonic deformation. LYAKHOVSKY et al. (1997a,b), HAMIEL et al. (2004) and references therein developed a thermodynamically-based continuum damage model for evolving elastic properties of rocks sustaining irreversible brittle deformation. The employed damage rheology is applicable to volumes with a sufficiently large number of cracks that allow quantitative description through properties of the crack distribution rather than those of the individual cracks (LYAKHOVSKY and MYASNIKOV, 1984, 1985). The model generalizes the strain energy function of a solid to account for first-order macroscopic effects of distributed cracks (i.e., damage), and makes the elastic moduli functions of an evolving damage state variable α representing the local crack density. An undamaged material with $\alpha = 0$ is the ideal solid governed by 3-D linear elasticity, while a material with $\alpha = 1$ is completely destroyed. Using the balance equations of energy and entropy, the damage model quantifies the effective elastic behavior of a cracked solid for all intermediate values of the damage variable ($0 < \alpha < 1$). Detailed reviews and recent developments of the model can be found in BEN-ZION and LYAKHOVSKY (2006) and LYAKHOVSKY and BEN-ZION (2008). Here we only summarize the main ingredients of the model that are relevant for our work.

The effects of distributed cracks (i.e., existing damage) on the elastic properties of a solid are accounted for in the damage model by generalizing the strain energy function to the form:

$$U = \frac{1}{\rho}\left(\frac{\lambda}{2}I_1^2 + \mu I_2 - \gamma I_1\sqrt{I_2}\right) \tag{1}$$

where $I_1 = \varepsilon_{kk}$ and $I_2 = \varepsilon_{ij}\varepsilon_{ij}$ are the first and second invariants of the elastic strain tensor ε_{ij}, ρ is the mass density, λ and μ are the Lamé parameters, and γ is a third modulus of a damaged solid. The first two terms of equation (1) give the classical strain potential of linear elasticity (e.g., MALVERN, 1969). The third term may be derived using the effective medium theory of BUDIANSKY and O'CONNELL (1976) for non-interacting cracks that dilate and contract in response to tension and compression (LYAKHOVSKY et al., 1997b), or by expanding the strain energy potential as a general second-order function of I_1 and I_2 and eliminating non-physical terms (BEN-ZION and LYAKHOVSKY, 2006).

The kinetic aspects of the damage rheology involve making the elastic moduli functions of the damage state variable, and deriving an equation for the evolution of

damage. LYAKHOVSKY *et al.* (1997a) showed that the leading term of the damage evolution equation, satisfying energy conservation and nonnegative entropy production, can be written as

$$\frac{d\alpha}{dt} = \begin{cases} C_d I_2(\xi - \xi_0), & \text{for } \xi \geq \xi_0 \\ C_1 \cdot \exp\left(\frac{\alpha}{C_2}\right) I_2(\xi - \xi_0), & \text{for } \xi < \xi_0 \end{cases} \qquad (2)$$

where $\xi = I_1/\sqrt{I_2}$ is referred to as the strain-invariants ratio, and C_d, C_1, C_2 are damage rate parameters further described in Sections 3.2 and 4.1. The parameter ξ_0 is a yielding threshold separating states of deformation involving material degradation ($d\alpha/dt > 0$) when $\xi > \xi_0$, and material healing ($d\alpha/dt < 0$) when $\xi < \xi_0$. AGNON and LYAKHOVSKY (1995) and LYAKHOVSKY *et al.* (1997a) related this parameter to the angle of internal friction by considering the critical shear stress for Mohr-Coulomb sliding. They obtained $\xi_0 = -0.8$ for rock with internal friction coefficient of $f = 0.6$ and Poisson's ratio $v = 0.25$, and noted that this value varies only slightly (-0.7 to -0.9) for rocks with Poisson's ratio between 0.2 and 0.3.

Equation (2) was derived assuming for simplicity

$$\begin{aligned} \lambda &= \lambda_0 = \text{constant}; \\ \mu &= \mu_0 + \alpha \gamma_m \xi_0; \\ \gamma &= \alpha \gamma_m; \end{aligned} \qquad (3)$$

where γ_m is the maximum value of the third elastic modulus defined by normalization of the damage variable. The dependencies of elastic moduli on the damage variable produce the following changes during loading: As the damage variable α increases, the shear modulus μ decreases, Poisson's ratio v increases, and the modulus γ increases from 0 (damage free) to γ_m. Following the onset of positive damage evolution above the elastic limit at $\xi = \xi_0$ and before the final macroscopic failure, the model incorporates a gradual accumulation of inelastic strain, ε_{ij}^v, described in Appendix 1. When the damage variable reaches a critical value α_{cr}, there is brittle instability leading to rapid conversion of deviatoric elastic strain to permanent plastic strain. The reduced deviatoric stress at the end of the brittle failure episode typically leads to a state $\xi < \xi_0$ that is associated (equation (2)) with healing. The exponential dependency of the damage recovery (healing) is motivated by the logarithmic healing with time that is observed for rocks and other materials (e.g., DIETERICH, 1978; 1979). LYAKHOVSKY *et al.* (2005) showed that the above damage model reproduces the main observed features of rate- and state-dependent friction, and constrained the healing parameters C_1, C_2 by comparing model calculations with lab Frictional data.

The main components of the numerical procedure, utilizing the Fast Lagrangian Analysis of Continua (FLAC) algorithm (e.g., CUNDALL and BOARD, 1988; POLIAKOV *et al.*, 1993), is presented in Appendix 1. To simulate long-term deformation processes with appropriate boundary conditions at the edges of our model domain, we use boundary conditions with variable forces (LYAKHOVSKY and BEN-ZION, 2008). These boundary

conditions account for the stress buildup and abrupt drop during each seismic cycle, and for the evolution of elastic properties and cumulative plastic strain within the model domain. Appendix 2 presents an overview of the variable-force boundary conditions, and Appendix 3 applies the conditions in a test study verifying the viscoelastic component of our code. Additional details on the employed damage model and comparisons of results with laboratory fracture and friction data are given by LYAKHOVSKY et al. (1997a,b, 2005), HAMIEL et al. (2004, 2006), BEN-ZION and LYAKHOVSKY (2006) and LYAKHOVSKY and BEN-ZION (2008).

3.2. Damage Model Parameters

A fundamental set of results of previous damage-based models is that rheological damage parameters have significant impact on the evolving geometrical properties of fault zones, seismicity patterns and spatial distribution of deformation. LYAKHOVSKY et al. (2001) and BEN-ZION and LYAKHOVSKY (2006) suggested that damage zone structure is primarily controlled by (1) the ratio between loading rate and healing rate, (2) the overall degree of "brittleness" of crustal deformation which may be parameterized by the seismic coupling coefficient χ, and (3) the susceptibility to propagation of rupture associated with dynamic weakening and related dynamic time scale τ_r. Below we review the main material parameters and outline their effect on fault zone evolution. Table 1 presents a synthesis of the plausible range of values for each parameter, and justifications for these values.

As discussed in the context of equation (2), the employed damage rheology includes three material parameters that affect the rate of damage evolution with time: C_1 and C_2 are both healing rate parameters, and C_d is the damage accumulation rate parameter. In our simulations, the loading rate is closely linked to the specified tectonic strain rate and the value of C_d is fixed. Therefore the ratio of loading rate to healing rate is governed by the healing rate parameters C_1 and C_2. Simulations with high healing rates compared to the loading rate result in rapid near-complete healing of fault damage. In such settings, ruptured fault zones quickly regain their strength, enabling larger interseismic stress accumulation and coseismic stress drops, and the evolving fault zones have more complex geometries than cases with low healing rates.

The degree to which crustal deformation is brittle is controlled by the material parameter C_v, the coefficient of damage-related inelastic deformation (Appendix 1). This material parameter determines the ratio of aseismic to seismic components of deformation, or the seismic coupling coefficient, given (BEN-ZION and LYAKHOVSKY, 2006) by $\chi = 1/(1 + R)$ through the nondimensional R value with $R = \mu_0 C_v$ and μ_0 being the initial rigidity of the material. LYAKHOVSKY and BEN-ZION (2008) demonstrated that higher crustal C_v values induce larger components of aseismic deformation in the seismogenic zone, and therefore lower coseismic stress-drops. The susceptibility to rupture propagation determines the degree of dynamic weakening and dynamic time scale τ_r during the occurrence of brittle instability. LYAKHOVSKY et al. (2001) found that higher

Table 1

Damage rheology parameters and their constraints.

Parameter	Preferred range	Justification for value, and references	Comments
C_d Damage accumulation rate	0.5–5 s^{-1}	Lyakhovsky *et al.* (1997a): Fracture experiments with granite at relatively high confining pressure (100 MPa)	Lyakhovsky *et al.* (2005) show that at shallow depths ($z < -5$ km) C_d increases with the decrease in confining pressure ($C_d^{surface} > 10$ s^{-1})
C_1, C_2 Healing rate parameters	$C_1 = 10^{-24}$–10^{-4} s^{-1} $C_2 = 0.1$–0.01	Lyakhovsky *et al.* (2005): Analysis of 1-D damage and comparison with rate and state dependent friction parameters	See discussion and new constraints in Section 4
ξ_0 Critical strain invariant ratio (generalized internal friction)	-0.7 to -1	Agnon and Lyakhovsky (1995): Analytic analysis indicates that a friction coefficient of $f \sim 0.6$–0.7 corresponds to $\xi_0 = -0.8$ Lyakhovsky *et al.* (1997a): 3-D faulting experiments yield $\xi_0 = -0.7$ to -1	Lyakhovsky *et al.* (1997a) also indicate a week dependency of ξ_0 on Poisson's ratio, ν, but concluded that $\xi_0 = -0.8$ for various rocks with $\nu = 0.2$–0.3
C_v Damage-related inelastic strain accumulation	10^{-4}–$5 \cdot 10^{-6}$ MPa^{-1}	Yang and Ben-Zion (2009): Analysis of aftershock sequence in southern California, and comparison to damage rheology predictions	1. C_v: $d\alpha/dt$ is the damage related compliance 2. Based on these C_v values, the fraction χ of elastic strain released during a seismic cycle as brittle deformation is estimated to be 30%-85%
τ_r Characteristic time scale for seismic wave damping	$3 \cdot 10^2$–$3 \cdot 10^4$ s	Ben-Zion and Lyakhovsky (2006): Largest aftershock magnitude analysis (comparing numeric results and expected log-linear relation)	

τ_r values induce larger ruptures and lead to relatively simple failure histories consisting of system-sized events occurring in a single fault zone.

The above material parameters are currently constrained mainly by analytical considerations and by fracture and friction experiments (Table 1). In the next section, we use geophysical data to narrow the admissible range of healing rate parameters, and to better relate these parameters to natural deformation processes observed along active fault systems.

4. Geophysical Constraints on Healing Rate Parameters

4.1. Parameters C_1 and C_2, and Healing as a Function of Time

As follows from equation (2), the healing rate depends on the strain magnitude (I_2), strain invariant ratio (ξ), level of material damage (α), and material properties including critical strain invariant ratio (ξ_0) and two healing rate parameters C_1 and C_2. The critical strain invariant ratio is well constrained and fairly constant ($\xi_0 \approx -0.8$). The strain invariants ratio (ξ) varies from $-\sqrt{3}$ to $+\sqrt{3}$. The post failure shear strain (I_2) is mostly controlled by the lithostatic pressure and may vary with depth by two orders of magnitude or less. Therefore, the rate and the overall effectiveness of the healing process are primarily determined by the rate parameters C_1 and C_2. While C_2 determines the rate dependence on the damage state α and varies within one order of magnitude, C_1 may vary by many orders of magnitude (LYAKHOVSKY *et al.*, 2005). Depending on the combination of these parameters the healing process may be fast or slow, and may yield insignificant or near-complete healing of the damaged material over long timescales. Equation (2) indicates that very large C_1 corresponds essentially to zero memory, in which case damaged material heals rapidly and almost completely. If damage accumulation is also rapid (C_d is very large) the model will display ideal elastoplastic behavior. Very small C_1 yields insignificant healing except for the special case of $C_2 \approx 0$ in which healing is near instantaneous and complete. Extremely large C_2 values lead to a healing rate proportional to C_1 (i.e., $d\alpha/dt = C_1 I_2 (\xi - \xi_0)$). In such cases, for $C_1 < 1 \cdot 10^{-10}$ s^{-1} the healing is slow and insignificant while for $C_1 > 1 \cdot 10^{-05}$ s^{-1} the healing is fast and almost complete (Fig. 1).

To better understand the healing process and constrain the parameters C_1 and C_2, we define a time scale for healing (τ_h) during which the relative change of the elastic moduli (μ, γ) is above an arbitrarily chosen rate of 0.1% yr^{-1} ($d\alpha/dt = 3 \cdot 10^{-11}$ sec^{-1}). Simplifying equation (2) for a uniform strain invariant ratio suitable for healing, assuming ($\xi - \xi_0$) to be of the order of one, and setting the healing rate to this chosen threshold, the expected damage level is given by

$$\alpha_f = C_2 \ln\left[3 \cdot 10^{-11}/C_1 I_2\right], \tag{4}$$

where α_f is the damage level as the healing becomes slower than 0.1% yr^{-1}. This value is referred to hereafter as the final damage level, even though slow although possibly
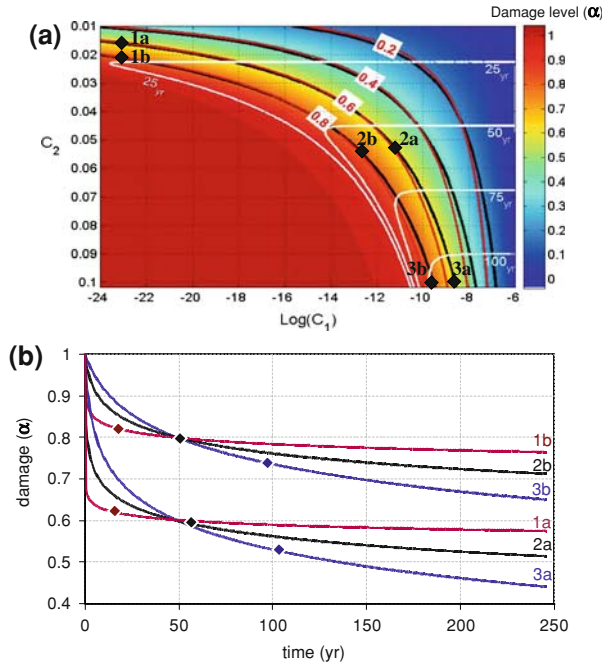
Figure 1

(a) Damage levels of typical crustal material at 10 km depth after 50 years of healing, for the damage model parameter space suggested by LYAKHOVSKY *et al.* (2005). Black and red lines show contours of equal damage and final damage (α_f), respectively. White lines are contours of equal healing time scale (τ_h). Black diamonds indicate sets of healing parameters referred to in Figure 1b. (b) Damage as a function of time after failure for six sets of C_1 and C_2 parameters (indicated in Fig. 1a). The healing time scale (τ_h) and final damage level (α_f) of each healing process are indicated by diamonds (red – 1a,b; black- 2a,b; blue – 3a,b). Note that some healing occurs after α_f is attained (see Section 4.1).

significant healing continues after α_f is reached (at geological time scales). Substituting α_f in equation (8) of LYAKHOVSKY *et al.* (2005) for the damage level as a function of time, the time scale for healing (i.e., the duration required to reduce the damage level from $\alpha = 1$ to α_f) can be estimated by

$$\tau_h = \frac{\exp\left(\frac{1-\alpha_f}{C_2}\right) - 1}{I_2 \frac{C_1}{C_2} \exp\left(\frac{1}{C_2}\right)}. \tag{5}$$

Within the healing parameter space that represents materials that undergo significant healing (i.e., damaged materials with $\alpha_f < 0.8$), the time scale for healing (τ_h) falls in the range 10–110 yr (Fig. 1a). The time scale for healing indicates how fast a damaged material heals to a near constant damage level, however it does not reveal the final damage level. Therefore, materials with similar τ_h may exhibit a wide range of final damage levels (Fig. 1). Figure 1b displays six healing processes determined by six sets of

C_1 and C_2 parameters (marked and labeled in Fig. 1a). Healing processes with short time scales (e.g., 1a and 1b in Fig. 1b) display higher initial healing rate and faster decay of the healing rate compared to processes with longer time scales (e.g., 3a and 3b in Fig. 1b). As evident from Figure 1b, in order to fully determine the healing parameters of a material one would either need to establish the damage level at two distinct times after failure or to determine the current damage level, the duration since failure and the healing time scale relevant to the specific healing process.

LYAKHOVSKY et al. (2005) suggested that the parameter C_2 is closely related to the parameter b of rate and state friction ($b \sim 10^{-1}$; $C_2 \sim 10^{-2}-10^{-1}$), and obtained the following relation between parameters C_1 and C_2:

$$C_1 \approx BC_2 \exp\left(-\frac{\alpha_0}{C_2}\right) \Big/ \varepsilon_{cmp}^2, \tag{6}$$

where B (~ 1–2 s^{-1}) is a laboratory-determined time scale for the evolution of static friction with hold time (DIETERICH, 1972, 1978) and ε_{cmp} is the compaction strain estimated by the ratio between lithostatic stress and the bulk modulus (K). LYAKHOVSKY et al. (2005) estimated $\varepsilon_{\text{cmp}} \sim 10^{-2}$ for crustal rocks at seismogenic depths, but noted that this strain level may vary significantly for various lithologies and depths. Since the lithospheric stress within the seismogenic zone (depth 1–20 km) ranges between 20 MPa and 400 MPa, and the bulk modulus of typical crustal rocks varies by an order of magnitude (CHRISTENSEN and MOONEY, 1995), it is safe to assume that the compaction strain could vary by 2–3 orders of magnitude. Given that the parameter B may differ from the well-constrained lab-based values and that compaction strain may vary significantly, we consider (Fig. 2) a wide range of C_1 values per C_2 value (six orders of magnitude).

4.2. In Situ Geophysical Constraints for Healing Parameters C_1 and C_2

We use data from seismic surveys along large fault zones with significant fault-related damage to better constrain the healing parameters C_1 and C_2. Simplifying equation (3) for uniform shear deformation $\mu = \mu_0(1-\alpha)$, and using the relation between rigidity, density and shear wave velocity ($\mu = \rho V_s^2$), we convert reported seismic velocity and rigidity reductions (Section 2) into damage level estimates. The seismic and geodetic studies indicate that major strike-slip fault zones rapidly heal in the top few km to $\alpha \approx 0.75$ during the early postseismic stage (BEN-ZION et al., 2003; PENG et al., 2003; LEWIS et al., 2005), and thereafter display damage levels of $\alpha > 0.5$ (HAMIEL and FIALKO, 2007; FIALKO et al., 2002; FIALKO, 2004). While the healing at greater depth is expected to be higher, these observations may indicate that damage zones of large active faults do not completely heal over time scales of typical earthquake cycles. This argument is supported by the abundance of ancient fault zones that remain weaker than the surrounding rock (TCHALENKO, 1970; SENGOR et al., 2005; ARMIJO et al., 1996; POWELL and WELDON, 1992; EVANS et al., 2000). Additional support comes from previous numerical models (LYAKHOVSKY et al., 2001; FINZI et al., 2006) and experimental work (TENTHOREY et al.,
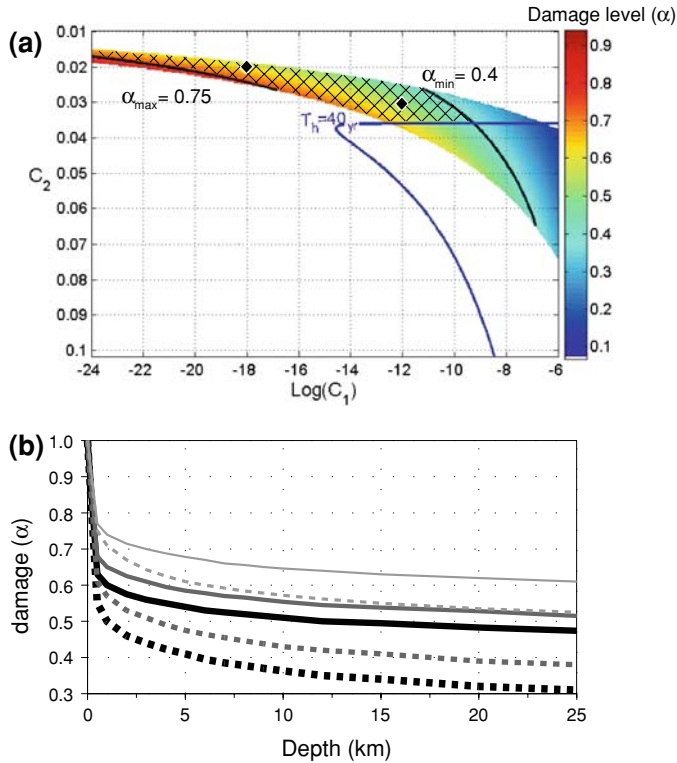
Figure 2

(a) Geophysical, analytical and laboratory-based constraints on healing parameters. Damage levels at a depth of 1 km after 50 years of healing are shown for C_1 values within three orders of magnitude of their expected values (Eq. (6)). The hatched region bracketed by the maximum healing time scale ($\tau_h = 40$ yr) and the minimum and maximum admissible damage levels ($0.75 > \alpha_f > 0.4$) represents the healing parameters relevant to models of natural damage zones (see text). Diamond symbols indicate two healing parameter sets plotted in Figure 2b for illustration. (b) Estimated damage versus depth after 0.1 yr (gray lines), 10 yr (dark gray lines) and 100 years of healing (thick black lines) under lithospheric stress conditions, for healing parameters representative of natural fault zones (solid lines: $C_1 = 1 \cdot 10^{-18}$ s^{-1}, $C_2 = 0.02$; dashed lines: $C_1 = 1 \cdot 10^{-12}$ s^{-1}, $C_2 = 0.03$).

2003) showing that damage zones do not heal completely during the earthquake cycle. The above is expected to be valid for low-porosity crystalline rocks. In contrast, deformation bands in sandstones and other high porosity rocks are frequently denser and stronger than their host rock (AYDIN and JOHNSON, 1983; SHIPTON and COWIE, 2003). The limited healing argument implies that long-term interseismic healing in low porosity rocks is typically minor and that damage generation and healing in such rocks occurs predominantly in the seismogenic crust during the co- and early postseismic interval (e.g., over weeks to months). This is supported by various postseismic healing rate studies (e.g., LI *et al.*, 2006; KARABULUT and BOUCHON, 2007; PENG and BEN-ZION, 2006; SCHAFF and

Beroza, 2004; Rubenstein and Beroza, 2004; Baisch and Bokelmann, 2001; Wu *et al.*, 2009).

We note that the similar interseismic damage levels for the different fault zones mentioned above may reflect resolution limitations of the seismic and geodetic methods (i.e., perhaps materials with $\alpha < 0.5$ are not reliably detected by these techniques). If this is the case, the argument that long-term healing is minor may not be valid. Furthermore, the healing parameters may be pressure- and/or temperature-dependent (as the damage accumulation rate parameter C_d). Further work should be done to better constrain the healing parameters at seismogenic depths. Finally, the healing computations in our parameter space study do not take into account ongoing deformation (and damage accumulation) due to continuous tectonic loading or nearby earthquakes, and therefore they may underestimate damage levels in natural systems.

Based on the above considerations we suggest two general constraints for the healing parameters suitable for models of natural processes: (a) the minimum damage level expected in shallow crustal fault zones during the interseismic stage should be above $\alpha \approx 0.4$, and (b) the healing time scale representative of natural damage zones should be shorter than $\tau_h \approx 40$ yrs (yielding healing rates of 5–10% yr^{-1} after 4–5 months of healing, and a very low rate of approximately 0.1% yr^{-1} after 40 years of healing). The resulting healing parameter space is outlined in Figure 2 by a hatched pattern. The admissible values of C_1 and C_2 in that subspace are 10^{-24} s^{-1} to 10^{-10} s^{-1} and 0.015 to 0.035, respectively.

A final analytical constraint for healing parameters can be derived from the convexity condition for macroscopic failure used in our damage rheology framework (Lyakhovsky *et al.*, 1997a). This stability condition indicates that near the surface, where normal stress is low compared to shear stress and the strain invariants ratio is approximately zero, the maximum sustainable (stable) damage level is approximately $\alpha = 0.75$. Therefore, healing parameters that yield lasting damage levels greater than $\alpha = 0.75$ at shallow depths ($z < 3$ km) are assumed to be nonrealistic (Fig. 2).

5. Damage and Strain Distribution across Active Strike-slip Faults

To investigate the structure of damage zones associated with evolving strike-slip fault systems, we use several realizations of a three-dimensional model of transform plate boundary incorporating damage rheology in the upper crust.

5.1. Model Setup

A typical model setup (Fig. 3) consists of a layered seismogenic crust governed by damage rheology, underlain by viscoelastic lower crust and upper mantle layers. The modeled region is 100–250 km in the along-strike direction, 100 km wide and 50 km deep. A detailed description of such a model setup is given by Ben-Zion and Lyakhovsky
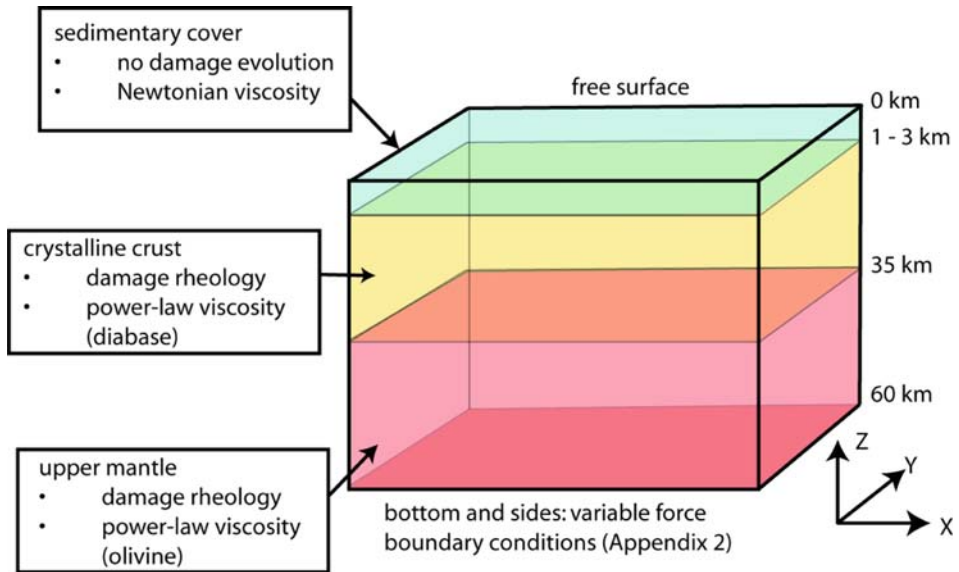
Figure 3

A block diagram of typical 3-D lithospheric structure used in the numerical simulations. The fault parallel extent of the model domain varies from 100 to 250 km in different simulations. Imposed damage (not shown in Fig. 3) is applied only in a few simulations of long-term fault stepover evolution (i.e., initial conditions of high-resolution fault stepover models included damage zones representing a segmented fault).

(2006). Here we only summarize the main ingredients. A diabase flow law is used to represent the rheology of the crystalline crust (CARTER and TSENN, 1987) and a dunite/olivine flow law is used for the upper mantle (KIRBY and KRONENBERG 1987). We assume a geothermal gradient of 20 C km^{-1}. The assumed flow laws and geotherm are kept fixed in our simulations. A range of damage model parameters, chosen from the values given in Table 1, is used in the models (Table 2). Since we are not trying to characterize surface damage structures, and as frequent failure of surface elements due to low confining stress would be computationally time consuming, we suppress damage accumulation in the simulated surface layer (typically top 3 km of the crust) by setting there $C_d = 0$. However, based on test models with $C_d > 0$ within the surface layer (not presented here), we expect that the surface damage zone is slightly wider and consists of locally higher damage levels than the underlying (simulated) damage zone.

A variable force boundary condition (LYAKHOVSKY and BEN-ZION, 2008, 2009) is applied to the sides and bottom of the model domain, simulating a constant far-field fault-parallel velocity with relative rate of 32 mm/yr (corresponding to the San Andreas Fault). These boundary conditions are further discussed in Appendix 2. The boundary driving forces are set to represent imposed fault zones outside the model domain, and they induce faulting near the centers of the north and south edges of the model (see for illustration Fig. A1). The top model boundary is stress free.

Table 2

Model parameters used in our fault evolution study (omitting models repeated with near-identical parameters)

Model name	Grid spacing (km)	Healing C_1 (s^{-1})	Healing C_2	Dynamic weakening τ_r	Seismic ratio χ	Initial damage heterogeneity	Initial τ_r heterogeneity
NB_0	3.2	6.0E-11	0.07	1.0E + 4	80%	0%	30%
NB_2	3.2	1.0E-13	0.02	1.0E + 4	80%	0%	30%
NB_6	2.2	1.0E-13	0.02	5.0E + 3	61%	0%	30%
NB_7	2.2	1.0E-13	0.02	5.0E + 3	99%	0%	30%
Nb_1_lap	3.2	1.0E-13	0.02	1.0E + 4	80%	0%	30%
Nb_3_lap	3	1.0E-13	0.02	1.0E + 4	80%	0%	30%
Nb_5_lap	2.2	1.0E-13	0.02	1.0E + 4	80%	0%	30%
Nb_7_lap	2.2	1.0E-13	0.02	3.0E + 3	67%	0%	30%
Nb_8_lap	2.2	1.0E-13	0.02	3.0E + 3	97%	0%	30%
Nb_9_lap	2.2	1.0E-13	0.02	5.0E + 3	57%	0%	30%
Nb_11_lap	2.2	5.0E-11	0.05	4.0E + 3	61%	0%	30%
Nb_geos_4	1.6	1.0E-13	0.02	1.0E + 4	80%	30%	30%
Nb_geos_6	1.6	1.0E-13	0.02	2.0E + 3	67%	30%	30%
Prop_2	3.2	1.0E-13	0.03	8.0E + 3	80%	25%	30%
Prop_7	3.2	2.0E-09	0.15	1.0E + 4	80%	15%	30%
Prop_9	3.2	6.0E-11	0.07	1.0E + 4	80%	25%	30%
Prop_lap_2	3.2	1.0E-13	0.03	9.0E + 3	80%	25%	30%
Prop_lap_6	3.2	1.0E-13	0.03	1.0E + 4	80%	10%	30%
Prop_run_a9	2.2	1.0E-12	0.03	5.0E + 3	61%	10%	30%
Prop_geos_5	2.2	1.0E-12	0.03	7.0E + 3	72%	10%	30%
Prop_lin_4.5	4.5	1.0E-13	0.03	1.0E + 4	80%	0%	30%
Stepover_8	0.25	1.0E-10	0.03	3.0E + 1	40%	100%	30%
Stepover_9	0.25	1.0E-10	0.03	1.0E + 2	40%	100%	30%
Stepover_10	0.25	1.0E-10	0.025	4.0E + 2	40%	50%	30%
Stepover_11	0.25	1.0E-10	0.025	6.0E + 2	40%	100%	30%
long-term_1	0.6	1.0E-12	0.03	6.0E + 4	80%	25%	30%
long-term_5	0.6	1.0E-20	0.02	6.0E + 4	80%	25%	30%

Other material parameters were set to represent crustal materials and were not varied in our models (these parameters include: ξ_o = -0.8. C_d = 5 s^{-1}; Sedimentary layer: density ρ = 2.4·10^{-3} Kg m^{-3}, Newtonian viscosity η = 10^{19} Pa S; Crustal rheology: Young's modulus E = 80 GPa, Poisson's ratio v = 0.3, ρ = 2.8·10^{-3} Kg m^{-3}, viscosity flow law coefficients: A = 6.3·10^{-20} Pa^{-n} S^{-1}, n = 3.05, Q = 276 Kj mol^{-1}; Mantle rheology: E = 150 GPa, v = 0.3, ρ = 3.3·10^{-3} Kg m^{-3}, A = 7.0·10^{-14} Pa^{-n} S^{-1}, n = 3.0, Q = 520 Kj mol^{-1})

5.2. Model Output: Examples and Interpretation

The model outputs include the level of damage α and strain ε. We calculate surface velocities, rigidity μ and other related quantities from these variables. Since α, ε and μ are computed throughout the model domain, both plan views (including depth slices) and cross-sectional views of these parameters may be plotted at any time step. Figures 4 and 5 show examples of model outputs, and illustrate features which correspond to observed geological structures such as fault segments, stepovers, and flower structures.

Contiguous sets of elements that fail repeatedly, resulting in a higher level of α (and a lower μ) than their surroundings, are interpreted as fault segments (Figs. 4, 5). Because of their relative weakness, these fault segments are also the centers of high velocity gradients
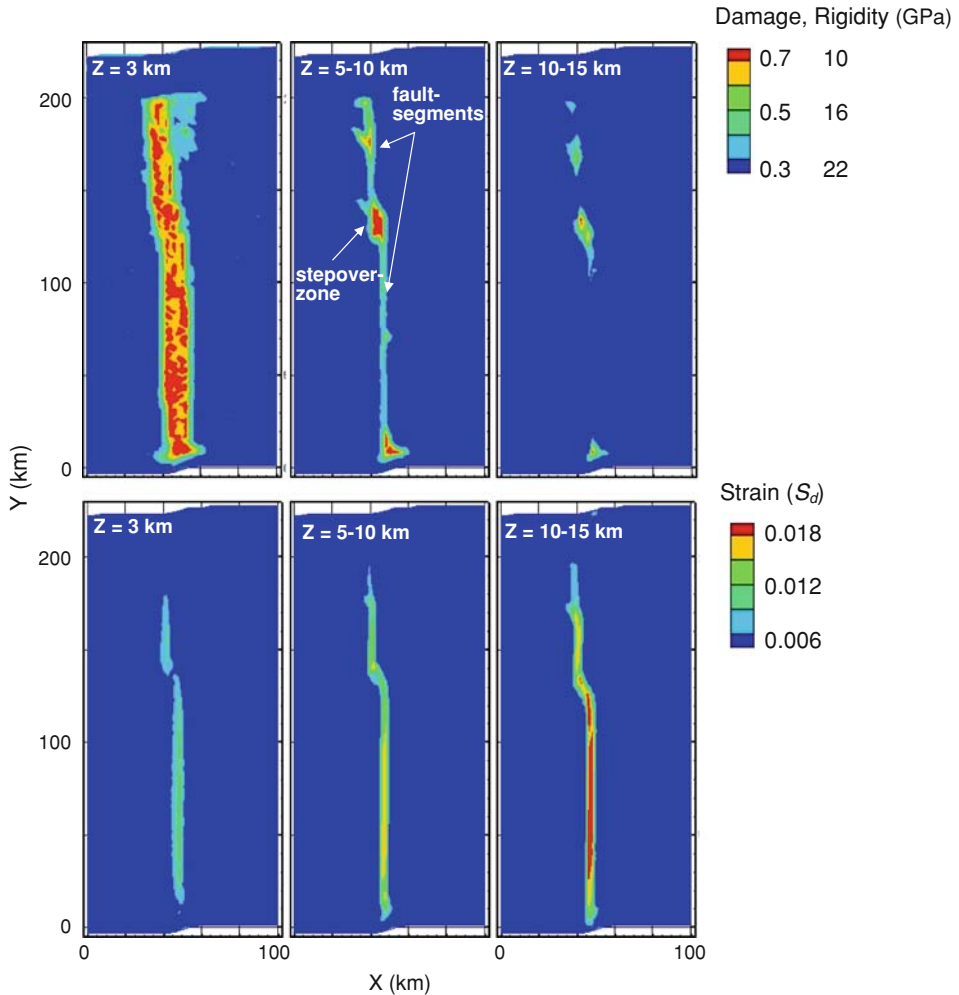
Figure 4

Plan views of a segmented strike slip fault at several depths, showing damage level (α), rigidity (μ) and the second invariant of the deviatoric strain, S_d ($S_d = \mathrm{sqrt}(e_{ij} \cdot e_{ij})$ where $e_{ij} = \varepsilon_{ij} - \delta_{ij} \varepsilon_{kk} /3$ and δ_{ij} is the Kronecker delta). Shallow ($z = 3$ km) damage (top left panel) is distributed within the stepover and around the fault segments. At depth ($z = 5$–10 km) damage is highly localized along the fault segments and is distributed within the fault stepover. At the lower part of the seismogenic crust, damage within stepover may persist long after the localized damage along fault segments heals.

and high strain rate (Figs. 4, 5). Cross-sectional profiles through modeled fault segments (Fig. 5) display "flower structures" with depth, which comprise localized damage along the active fault core with a superimposed, broader zone of distributed damage in the top 3–10 kilometers of the crust (Figs. 4, 5). Based on these observations, we define two damage subzones that are distinct in their evolution patterns, damage level, and spatial
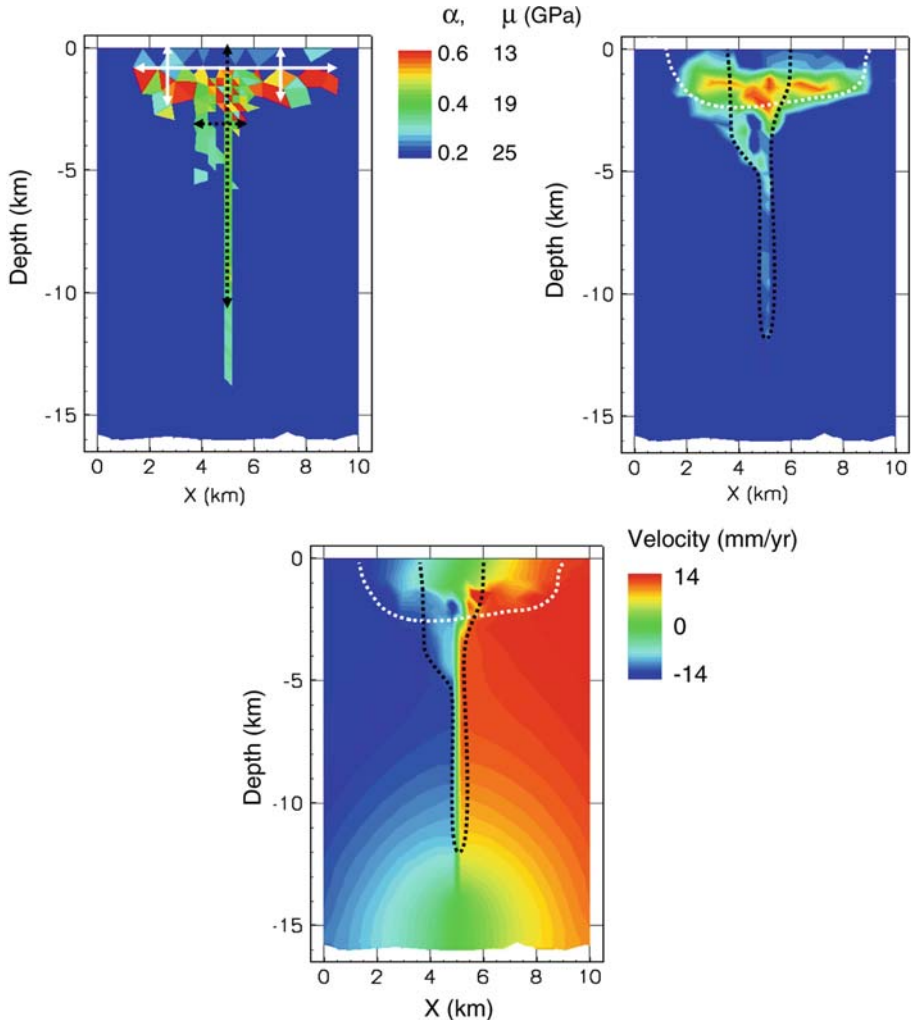
Figure 5

Cross-sectional views of a typical "flower type" damage zone along a strike-slip fault, displaying damage levels and rigidity (**A** and **B**), and fault-parallel velocity (**C**). Annotations in (**A**) show the dimensions of the Localized Active Fault (LAF) damage (black lines) and Distributed Off Fault (DOF) damage (white lines) as they were measured in this study. Dashed black and white lines show the location of the LAF and DOF damage zones (respectively) in the smoothed contour plots (**B**, **C**).

distribution: (1) Localized Active-Fault (LAF) damage which represents the highly localized damage along the active fault cores (Figs. 4, 5). The LAF damage is coseismically very high along the primary slip zone, but it rapidly heals at depth. (2) Distributed Off-Fault (DOF) damage which is sustained cumulative damage resulting from many earthquakes. The DOF damage develops during the early stages of
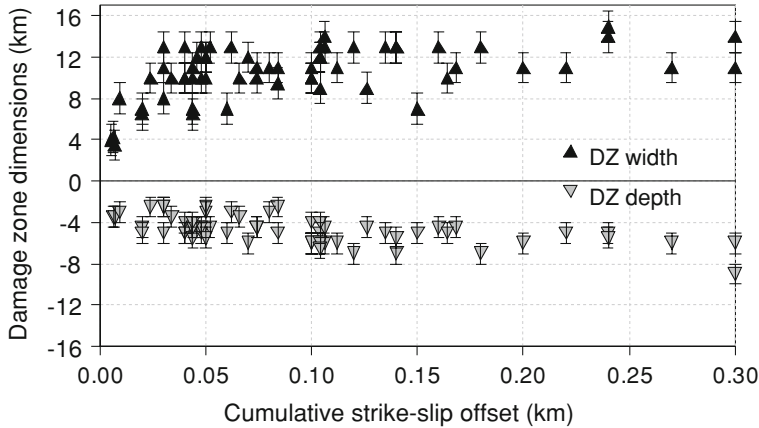
Figure 6

DOF damage zone width and depth plotted against cumulative strike-slip offset. After an initial stage with relatively fast damage zone growth, the DOF damage zone dimensions remain fairly constant (at offsets exceeding 0.05 km).

fault-system evolution, and thereafter its spatial extent is stable and the degree of damage within it evolves locally (Figs. 4, 5, 6). Descriptive analyses of damage structures along simulated strike-slip fault segments are given in Section 5.3.

Plan views of the model domain show several examples of stepover zones where segments are offset from one another (Fig. 4). Our models produce just extensional stepovers; that is, during propagation, new offset faults form in areas where end-effects from existing faults contribute a tensional mean normal stress. Stepovers are characterized by a wide DOF damage zone, and by high levels of damage, high strains, and low rigidity within the stepover. Descriptive analyses of damage structures within simulated stepover-zones are given in Section 5.4.

Before we discuss the results of our models, we need to (1) introduce observable quantities which may be systematically measured and then used to compare between model results, (2) define a threshold criterion for the maturity of our modeled faults to ensure that we base our analysis only on models that were run long enough to form mature damage zones, and (3) confirm that the model results presented here are fairly insensitive to numerical element dimensions. This is necessary because the models shown on Table 2 were run for different durations, and for a range of element dimensions.

To systematically describe the spatial extent of damage zones around faults we have chosen a threshold damage level of $\alpha = 0.35$ (presumably above any expected background damage level). The four quantities used to define the extent of damage are the widths and depths of both the LAF and DOF damage zones. Measurements of these quantities are performed on plan-view and cross-section plots of the simulated fault zones (without smoothing). The width of the DOF damage represents the maximal spatial extent of the damage zone, and its depth is the average depth extent of the shallow distributed

damage away from the active fault core (Fig. 5a). The width of the LAF damage represents the maximum width of the localized damage along the fault core, and its depth is the maximum depth extent of the damage zone (Fig. 5a). To facilitate comparison with geodetic studies we define also the Fault Compliant Zone (FCZ) in our models as the volume in which the average material rigidity is reduced by 50% relative to the host rock, consistent with the compliant zones of FIALKO *et al*. (2002). The simulated FCZ typically consists of the entire LAF damage and most of the DOF damage.

Strike-slip fault systems evolve over time, first becoming complex and then gradually simplifying to a more continuous configuration with fewer fault segments (e.g., BEN-ZION and SAMMIS, 2003 and references therein; LYAKHOVSKY and BEN-ZION, 2009). This complicates directly comparing model runs that may have been cut off at different evolutionary stages. Figure 6 illustrates that the width and depth of the DOF damage initially grows rapidly, starting to stabilize after a total relative displacement of approximately 0.05 km. This simulated stage of rapid DOF damage growth represents the initial stage of fault growth and complexity increase after which the fault configuration starts to stabilize and the strain localizes along the fault. Hence to analyze mature damage zone structures we can only use fault simulations with a total displacement larger than 0.05 km.

All results displayed on subsequent plots are for models with mature damage zones in which at least 0.05 km of displacement has accrued (corresponding to a modeled time interval of about 1600 years).

Since brittle failure in our simulations is associated with an abrupt transition from initial (static) to final (dynamic) stress levels, the numerical models are inherently discrete (e.g., RICE and BEN-ZION, 1996) and some aspects of the results are expected to be grid-dependent. An analysis of our entire set of damage zone simulations indicates that while the spatial extent of damage is somewhat grid-size dependent, the average level of damage within voluminous damage zones (e.g., stepover zones) is probably not grid-size dependent (Fig. 7). Furthermore, the spatial extent of damage zones in our models with element dimensions between 0.6 and 4 km (Fig. 7) are not significantly sensitive to element size. Results of models within this range of element dimensions will be shown together on subsequent plots. Models with finer and coarser elements were also run. For models with 4.5 km elements, results were smeared forming apparently wider and deeper damage structures. Models with 0.25 km elements ran very slowly and were numerically unstable. These simulations were terminated after 10–20 days of CPU time, during which the simulated damage zones did not reach a stable width. Based on Figure 6 we interpret the narrow and shallow damage zones that formed in these simulations as being immature, and we therefore do not incorporate them in our analysis.

5.3. Damage, Rigidity and Strain Distribution across Strike-slip Fault Segments

Simulated damage zones along strike-slip faults form flower structures consisting of a shallow DOF damage zone 6 to 14 kilometers wide and up to 7 kilometers deep, and a
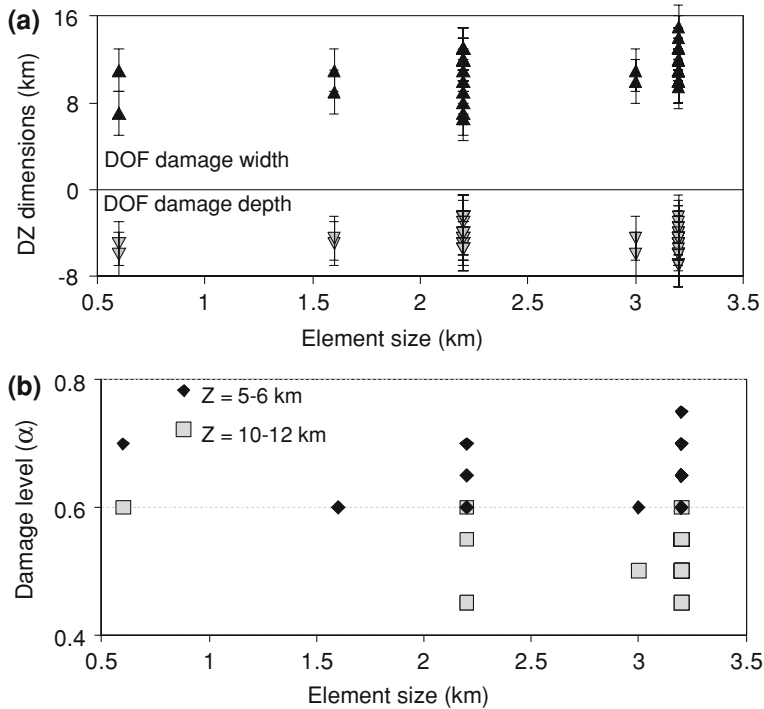
Figure 7

Sensitivity of model results to element size. (**a**) For models with element dimensions between 0.6 and 3.2 km, DOF damage zone dimensions are fairly insensitive to grid size. (**b**) Damage levels in fault stepovers at depth of 5–6 km and 10–12 km. These damage levels are insensitive to element size within the range we model. The scatter in results on both panels is due to different values of damage model parameters and variations in cumulative slip.

more intense LAF damage zone around the fault core. The DOF damage is the result of cumulative damage from past earthquakes (Figs. 5, 6). The LAF damage is narrow and steeply dipping, and it may extend to the bottom of the seismogenic zone (Figs. 4, 5) coseismically and in the early postseismic interval. The deeper parts of the LAF damage zone are only one model element wide and appear discontinuous (Figs. 4, 5). This probably indicates a tendency to evolve to a much narrower extent than our model element dimensions, in agreement with observed extreme localization of active slip zones (e.g., CHESTER and CHESTER, 1998; SIBSON, 2003; ROCKWELL and BEN-ZION, 2007). The highest damage levels along fault segments are usually found at the shallowest part of the LAF damage zone. The parts of the LAF damage in the shallow crust that are more than one element thick may correspond to the observed distributed DZ along the surface trace of large strike-slip faults.

The flower structure in our simulations is a robust feature that shows little dependence on damage parameters (C_1, C_2, χ, τ_r), and limited sensitivity to the presence of various
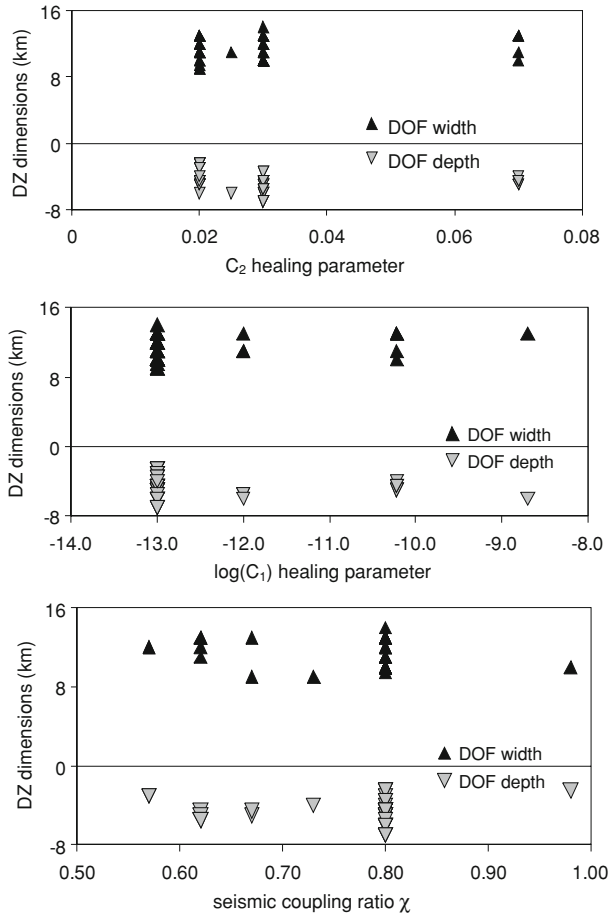
Figure 8
Width and depth of the distributed part of the damage zone (DOF damage) for models with a wide range of material parameters. DOF damage zone dimensions are insensitive to the healing parameters and the seismic coupling ratio.

degrees of material heterogeneities (Table 2). The insensitivity of the DOF damage to healing parameters (Fig. 8) may imply that the shallow crust is readily damaged and it experiences limited healing regardless of material parameters. This apparent insensitivity to the healing parameters may also indicate that the current range of modeled healing parameters is insufficient and further analysis is needed to understand the role of healing in damage zone evolution. The deeper sections of the LAF damage are more sensitive to the healing rate parameters (Fig. 9a). This reflects the fact that healing processes are sensitive functions of the normal stress. Our results indicate that the depth extent of the LAF damage (after the early postseismic interval) ranges from the entire seismogenic zone for materials with extremely slow healing ($C_2 > 0.05$; $\tau_h > 55$ yrs; Fig. 9b) to a few
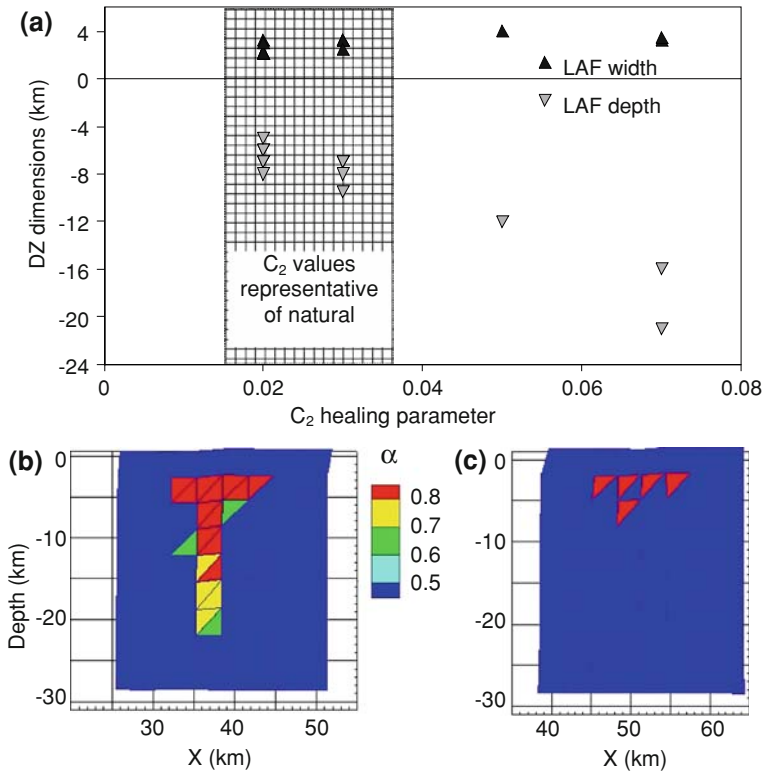
Figure 9

(**a**) Width and depth of the LAF damage zone as a function of healing parameter C_2 (width measured at 5–8 km depth, just below the DOF damage). The hatched region indicates admissible values of C_2 for modeling natural processes (see section 4). (**b, c**) Examples of deep and shallow fault core damage zones in models with long (**b**) and short (**c**) healing time scales. The geometry of these zones is stable through most of the interseismic interval.

kilometers for the faster healing materials ($C_2 < 0.03$; $\tau_h > 25$ yrs; Fig. 9c). Model realizations with healing parameters representative of natural processes (see Section 4) indicate that during most of the seismic cycle the contiguous well-developed LAF damage is limited to the top section of the crust (e.g., Figs. 9c, 10a). These results are consistent with numerical simulations of plastic strain generation during dynamic rupture (BEN-ZION and SHI, 2005), and analyses of large seismic data sets recorded around active faults (e.g., BEN-ZION *et al.*, 2003; PENG *et al.*, 2003; KORNEEV *et al.*, 2003; COCHRAN *et al.*, 2003; LEWIS e*t al.*, 2005; GRAYMER *et al.*, 2007).

The elastic strength of simulated fault zones is reduced as the damage level increases. The relation between rigidity and damage level (equation (2)) implies that the effective rigidity is primarily a function of α. However, the effective rigidity is further reduced near the surface and along the fault core because the strain invariants ratio ξ is higher at these
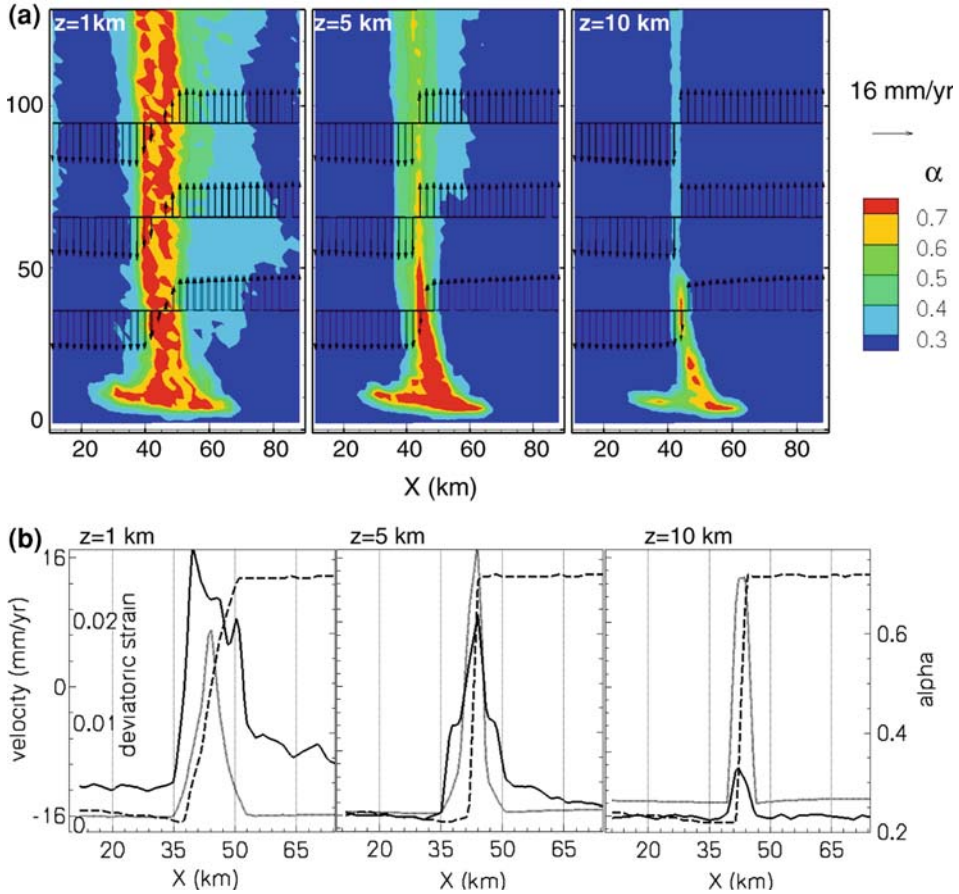
Figure 10

Correlation between damage and strain across simulated fault-zones. (**a**) Damage at depths 1, 5, 10 km and superimposed fault-parallel velocity. (**b**) Plots of damage level (solid curve, right ordinate), long-term (multi-cycle) fault parallel velocity (dashed curve, outer-left ordinate) and deviatoric strain (gray dotted curve, inner-left ordinate) for the same depths, extracted along the central section shown in (**a**) (at y = 65 km).

localities. Our damage zone models indicate that significant rigidity reduction (50–70% reduction) occurs within the shallow DOF damage and along the upper part of the fault-core (e.g., top 5 km of the LAF damage). Along the LAF at depths exceeding 12 km healing is rapid and the long-lasting (interseismic) reduction on μ is relatively small (Figs. 4, 5).

Our fault evolution models indicate that the bulk of inelastic strain is concentrated in the highly damaged cores of the fault zones (i.e., along the LAF damage). However, our models also exhibit low-gradient strain beyond the fault cores in the uppermost crust (top 3–5 km). The modeled off-fault strain is typically confined to a shallow layer approximately 10–15 km wide that exhibits significant DOF damage ($\alpha > 0.4$: see

Fig. 10). Where the shallow DOF damage is of lower intensity ($\alpha < 0.4$) our models do not display significant strain, suggesting that relatively thin layers of slightly damaged rock may not modify regional surface deformation patterns and may not be easily detectable by means of geodesy. At distances greater than 10 km from fully formed fault-zones, the total deviatoric strain is negligible and the long-term average strain rate is uniform, indicating that the undamaged upper crust behaves kinematically as a rigid block. The correlation between damage and strain distribution confirms recent interpretations of observed surface deformation patterns above fault-related compliant zones (e.g., FIALKO *et al.*, 2002; FIALKO, 2004). This correlation indicates that geodetically observed compliant zones are related to relatively high damage levels ($\alpha > 0.4$), and suggests that parts of the damage zones ($\alpha < 0.4$) may not be geodetically observable.

5.4. Fault Stepovers

While major fault segments display a positive feedback of strain-weakening and localization along highly damaged fault cores, persisting geometrical features such as fault offsets, kinks, and bends, may display strain-hardening and produce local complexity and new fractures at different scales (BEN-ZION and SAMMIS, 2003). In our models, segmented fault zones display continuous distributed seismic and aseismic deformation within fault stepover zones. This consists of aseismic strain and small earthquakes; however, moderate earthquakes ($M_L < 5.5$) also occur occasionally. While much of the damage along fault segments heals during the interseismic stage, the damage level at stepovers remains persistently high (Fig. 11a, compare with Fig. 9c). Fault stepovers and segment termination zones undergo significant damage accumulation during the interseismic stage, typically displaying average α between 0.5 and 0.75 (measured at a depth of 5–10 km), depending on the healing rate parameters. The damage within stepovers extends to greater depths than along fault segments, and in many simulations it reaches the bottom of the seismogenic zone (Figs. 11, 4). Models with realistic healing parameters typically exhibit significant damage ($\alpha > 0.5$) to depths of 10–15 km (Fig. 11). An important implication of the permanently elevated damage level within fault stepovers is that these regions of reduced μ (Fig. 4) affect rupture propagation and strong ground motion patterns.

5.5. Fault System Complexity as a Function of Time

According to our results, the DOF damage dimensions depend on the maturity of the fault system. Simulations with a wide range of material properties and numerical characteristics (e.g., element dimensions and boundary conditions) indicate that the damage zone grows until the fault accumulates an offset of about 0.05–0.1 km (Fig. 6). During this early evolutionary stage, the fault system's complexity increases as additional segments nucleate and propagate, forming new damage zones. This stage culminates as deformation localizes along narrow slip zones. As mentioned, an important exception to
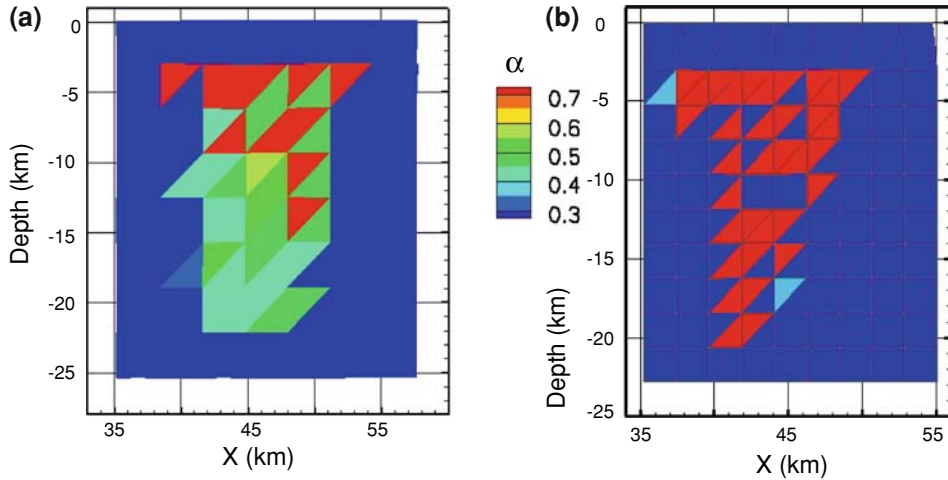
Figure 11

Cross-sections of damage patterns within fault stepovers. These zones of fault complexity are interseismically active, retaining high damage levels throughout the entire seismic cycle. Significant differences in damage level at depth (i.e., at Z > 10 km) arise from varying healing parameters: Models with fast and efficient healing (**a**) yield lower damage levels than those with slow and inefficient healing (**b**). Based on our healing rate analysis (Section 4), the faster healing models (e.g., **a**, and Fig. 9c) are better representatives of natural DZ processes. The healing rates in these models are identical to those in Figures 9b and 9c.

this evolution stage is the widening of the DZ at bends and stepovers and other local fault complexities (Figs. 12a-c, 13). The fault system evolution continues as through-going faults bridge sites of fault complexity such as stepovers (Figs. 12d, 13). When through-going faults fully form and bridge the entire depth of the stepovers, these structures may become inactive. After this stage the width and depth of distributed damage remain fairly constant, until the existing fault configuration cannot accommodate the evolving regional stress, at which point new faults form and migration of faulting may occur. Parallel faults may sustain simultaneous damage accumulation (Fig. 13) or exhibit alternating deformation periods before the initial faults become inactive and the new fault configuration stabilizes. These results are consistent with existing multi-disciplinary knowledge of fault systems (BEN-ZION and SAMMIS, 2003 and references therein; DOLAN et al., 2007) and the related numerical results of LYAKHOVSKY and BEN-ZION (2009).

6. Discussion and Conclusions

We perform a large numerical parameter-space study relating to general aspects of structural evolution of large strike-slip faults and related deformation fields, using a layered lithospheric model with an upper crust governed by a continuum damage rheology. One barrier to the widespread incorporation of damage rheology in crustal
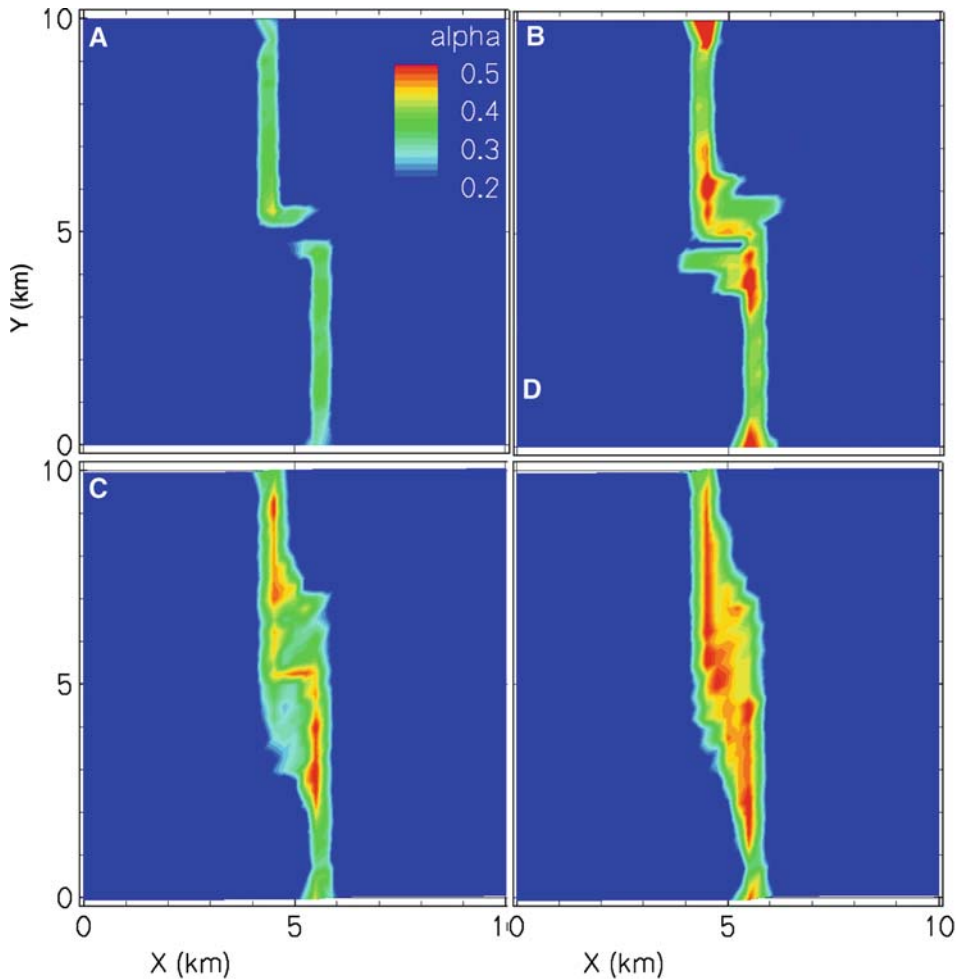
Figure 12

Fault stepover evolutionary stages displayed in four snap-shots of damage levels around a stepover zone (at 3 km depth). (**a**) Segmented fault. (**b**, **c**) Extensive damage accumulation within the stepover zone. In (**c**) distinct lateral (subsidiary) "faults" (regions of high damage) link between the two fault segments. (**d**) Formation of a through-going fault through the entire stepover zone. These results are from high-resolution, small-domain models focusing on stepovers.

deformation models has been the numerous damage model parameters, whose relationships with observable phenomena are sometimes unclear. Considerable work in recent years has gone into relating these parameters to results of brittle deformation experiments and thermodynamic theory (e.g., LYAKHOVSKY *et al.*, 2001, 2005; HAMIEL *et al.*, 2004, 2006). We take this further by using the observed shear modulus reduction in damaged fault zones to constrain the ranges of likely values for healing parameters C_1 and C_2. We find that admissible values of C_1 and C_2 are 10^{-24} to 10^{-10} s^{-1} and 0.015
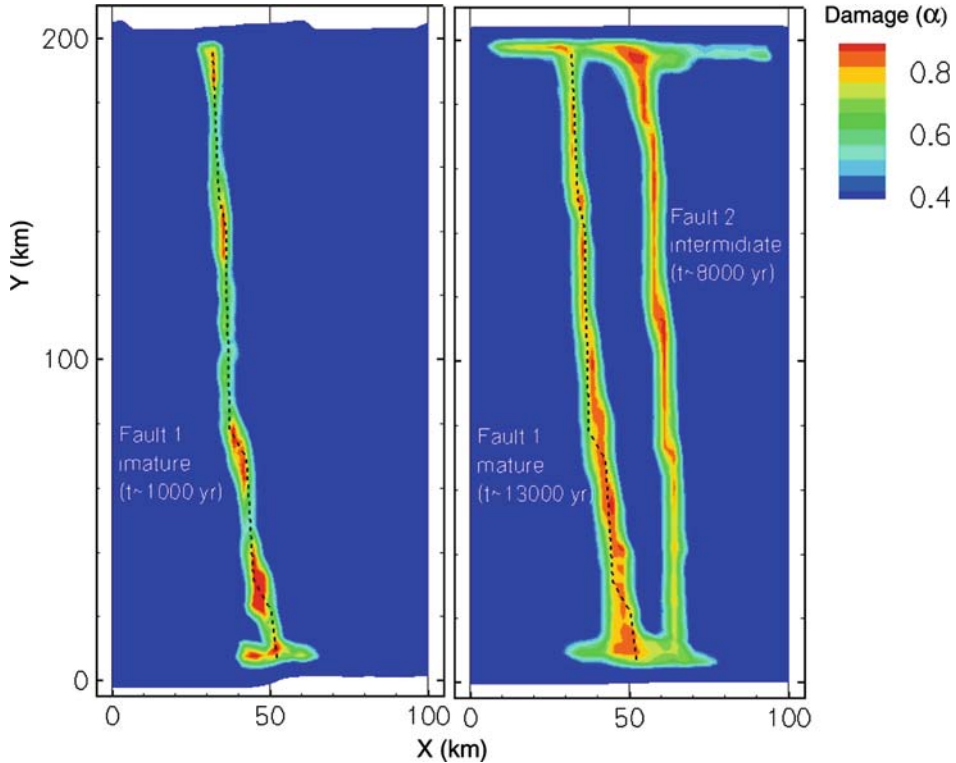
Figure 13

Fault evolution snap-shots showing damage levels at 10 km depth. The originally segmented fault (left panel; notice large stepovers) is smooth with time (right, mature fault 1; note that some of the apparent small stepovers are actually numerical artifacts formed because the fault is not parallel to the grid). An additional fault formed after approximately 5000 yrs to better accommodate regional stress (right, fault 2). Annotations of times in the images indicate the age of each fault in the simulation. Finely dashed line long fault 1 in both panels indicates its original segmented outline (as shown in left panel).

to 0.035, respectively (Fig. 2). This range is significantly reduced relative to previous studies (e.g., LYAKHOVSKY *et al.*, 2005).

Our models with reasonable damage and viscoelastic parameters yield general deformation patterns that are comparable to those seen in natural strike-slip fault systems. Flower structures, stepovers, localized strain around fault segments and permanent damage in the shallow upper crust and within stepovers are all reproduced. Due to model simplifications (e.g., no damage accumulation in the surface layer) and element size limitations, our models cannot conclusively predict the details of surface damage patterns, the width of the fault core, or the geometry of small faults and fractures within flower structures and stepover regions. Our simulations would probably yield narrower damage zones if we incorporated depth-dependent damage-rate parameters as suggested by LYAKHOVSKY *et al.* (2005).

The fault stepover zones in our models exhibit extensive damage and elasticity degradation sustained during many earthquake cycles. The simulated tensional stepovers show damage patterns consistent with intense tensile fracturing and dilation, and therefore are expected to exhibit long-lived enhanced permeability. Such damage patterns are consistent with recent structural evolution models for dilational stepovers (DE PAOLA *et al.*, 2007), and with mineral exploration studies that relate hydrothermal ore deposits to long-lasting extensive damage and increased permeability within fault stepovers (MICKLETHWAITE and COX, 2004; SHELDON and MICKLETHWAITE, 2007). The permanent damage zones our models predict should be detectable with detailed seismic and geodetic imaging studies.

An important implication of the predicted damage zones at stepovers concerns the interaction between damaged material and propagating earthquakes. During the interseismic stage, weakened stepover zones experience continuous earthquakes and proportionally more inelastic strain than the surrounding crust. This reduces the interseismic stress accumulation in the stepover region, which could aid earthquake rupture arrest. Various studies address rupture propagation across stepovers using quasi-static models (e.g., SEGALL and POLLARD, 1980), dynamic models (HARRIS and DAY, 1999; HARRIS *et al.*, 1991) and field observations (e.g., WESNOUSKY, 2006). Such studies show that it is easier for a rupture to jump across dilational stepovers (such as those our model produces) than compressional stepovers, because dilational normal stress brings nearby faults closer to failure. SIBSON (1985) and HAMIEL *et al.* (2005) argue, however, that during an earthquake, the normal stress change in a dilational stepover could lead to a sudden opening of fluid-filled cracks, reducing pore pressure and causing material hardening. An analogous effect is also seen in some of the models of HARRIS and DAY (1993), where fluid within a dilational stepover inhibits the ability of rupture to propagate across it. As long-term damage accumulation and coseismic pore pressure decrease have competing effects on the elastic strength of a stepover, further study will be required to clarify the ramifications of damage for rupture propagation and arrest. We also note that the extensive rock damage near stepovers should produce amplified ground motion, and hence higher seismic hazard, at those regions.

While the presented model simulations have several limitations, the following features appear to be robust:

- Distributed fault zone damage develops early in the evolution of a fault system (approaching steady-state damage zone dimensions after .05 km of total slip in our models).
- The strain generally localizes to narrow segments which are wider near the surface than at depth (representing flower structures).
- Along fault segments, the damage heals postseismically at depths exceeding 5–10 km and is permanent at shallower depths.
- The off-fault strain distribution correlates with the permanent shallow damage exhibited along fault-zones.

- Stepover regions may be permanently damaged to mid-crustal depths, and such damage zones should be detectable with focused seismic and geodetic studies.

Our numerical simulations of fault zone evolution suggest that the overall aspects of fault zone deformation along large faults at seismogenic depths can be modeled effectively over time intervals of several large earthquake cycles by a collection of narrow segmented zones or planar surfaces (i.e., without incorporating off-fault damage evolution). However, the evolving fault zone structures and off-fault damage play important roles in the evolution of geometrical properties of fault sections, the formation of fault systems, and in the deformation patterns along plate boundaries. Although regional scale static stress transfer in the crust is probably only moderately affected by the presence of shallow weakened damage zones along fault segments, long-lived volumes of extensively damaged material within fault stepovers and near other persistent geometrical irregularities can significantly affect earthquake propagation, strong ground motion, (locally) crustal stress state and surface deformation patterns.

Acknowledgments

Appendix 1: Numerical Procedure

The numerical code we use for our modeling utilizes the Fast Lagrangian Analysis of Continua (FLAC) method (e.g., CUNDALL and BOARD, 1988; POLIAKOV et al., 1993). This formulation is explicit in time and it continuously updates the shape functions of tetrahedral elements allowing large deformations to be simulated. The general procedure involves solving the equations of motion to determine nodal velocities and to calculate the elastic component of the element strains. The total strain tensor is calculated by summing the elastic strain component, a viscous strain component and a component representing the damage-related inelastic strain ε_{ij}^{v}. HAMIEL et al. (2004) introduced the gradual inelastic strain, ε_{ij}^{v}, whose accumulation rate is proportional to the rate of damage accumulation:

$$\frac{d\varepsilon_{ij}^{v}}{dt} = \begin{cases} C_v \dfrac{d\alpha}{dt}\tau_{ij} & \text{for } \dfrac{d\alpha}{dt} > 0 \\[2mm] 0 & \text{for } \dfrac{d\alpha}{dt} \leq 0 \end{cases} \tag{A1}$$
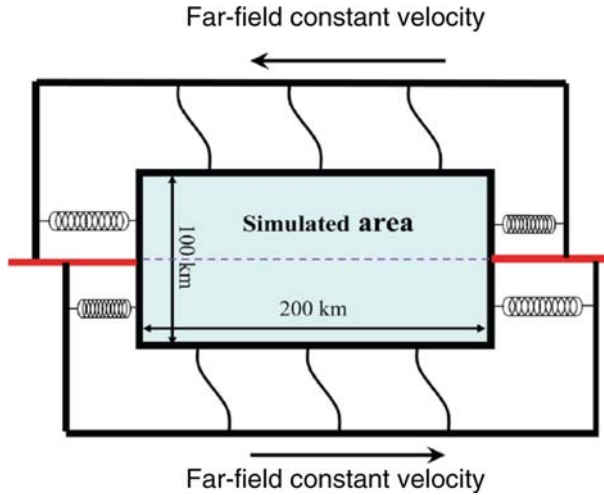
Figure A1

Schematic illustration of the variable force boundary condition. The model domain is coupled to a constant, fault-parallel velocity in the far-field, with the degree of coupling depending on a stiffness parameter (springs). Red lines indicate shear localization imposed by the boundary conditions as they were applied in our models (localized shear is also applied on the bottom boundary of our models, not illustrated here). Tectonic velocities and domain dimensions are for illustration and may be varied.

C_v is a material constant and $\tau_{ij} = \sigma_{ij} - \sigma_{kk}\delta_{ij}/3$ is the deviatoric stress tensor. The compliance, or inverse of viscosity ($C_v \cdot d\alpha/dt$), relates the deviatoric stress to the rate of irreversible strain accumulation. BEN-ZION and LYAKHOVSKY (2006) connected the rate of irreversible strain accumulation with partitioning between seismic and aseismic deformation in the seismogenic zone, and showed that the fraction of elastic strain released seismically, referred to as the seismic coupling coefficient χ, can be estimated as:

$$\chi = \frac{1}{1+R} \qquad (A2)$$

The damage rheology constitutive and kinetic relations provide element stresses and local values of damage, which are used to update material properties (moduli μ and γ) and to calculate the nodal force balances applied in the next time step. This procedure continues through many time steps until damage in any element reaches the critical level $\alpha = \alpha_{cr}$ associated with brittle instability. The brittle failure at any element may lead to rupture propagation. This is simulated with a quasi-dynamic procedure for calculating stress drop and plastic strain in regions sustaining brittle instabilities (LYAKHOVSKY and BEN-ZION, 2008). Their formulation connects the damage rheology parameters with dynamic friction of simpler frameworks, and the plastic strain accumulation is governed by a procedure that is equivalent to Drucker-Prager plasticity.
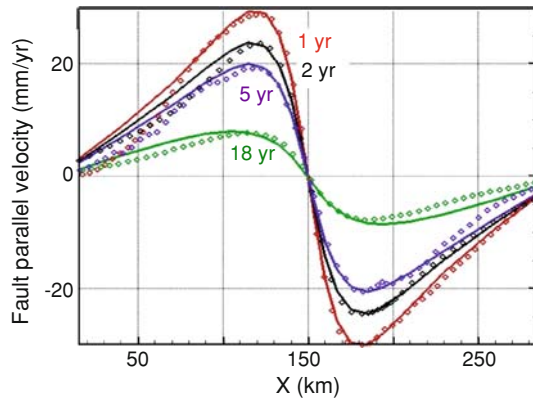
Figure A2
Surface velocities from our damage-disabled model (points) compared to a finite element solution of viscoelastic postseismic deformation (solid lines). The various lines and points represent velocities after 1 year (red), 2 years (black), 5 years (purple) and 18 years (green) of postseismic deformation. Maxwell time $T_m = 110$ years, other model detail are given in Appendix 2.

Appendix 2: Boundary Conditions

Numerical models of evolving fault systems typically incorporate either constant velocity or constant stress boundary conditions. LYAKHOVSKY and BEN-ZION (2008) show that these boundary conditions may generate very different velocity distributions during the interseismic period, and they conclude that neither of these boundary conditions is appropriate for simulations of fault system evolution over many earthquake cycles. To perform such simulations, LYAKHOVSKY and BEN-ZION (2008) introduced a modified boundary condition in which forces are proportional to a stiffness of virtual springs multiplied by the mismatch (slip-deficit) between the far-field plate motion and displacement of the boundary nodes (Fig. A1). Unlike the constant-velocity or constant-stress boundary conditions, this boundary condition accounts for stress accumulation and strain-rate decrease during the interseismic periods, as well as abrupt stress reduction at the model boundary during seismic events. The variable force condition realistically adjusts the forces applied on the model domain boundaries according to the evolution of elastic properties, stress state, and seismic events within the simulated domain (LYAKHOVSKY and BEN-ZION, 2008).

We constructed a series of test models to demonstrate the performance of this boundary condition and to study the spring stiffness parameter. Using these models we compared postseismic deformation in large domain models with fixed fault parallel boundaries, to results obtained from narrow-domain models with the variable force boundary condition. In the large models the domain width was set to be twenty times larger than the prescribed rupture depth (so that minor deformation is expected to occur near the fault parallel boundaries), and the fault-parallel boundaries were fixed. In the narrow-domain models, the fault perpendicular width was 140 km (i.e., fault parallel

boundaries were 70 km from the fault). In both the narrow- and wide- domain models the rheology was set to be viscoelastic without damage evolution, and with realistic material properties ($\mu = 30$ GPa, $v = 0.25$, elastic plate thickness 20 km, and Newtonian substrate viscosity of 10^{19} Pa s). The analysis of stiffness values and their effect on boundary forces and velocities shows that using a very large spring stiffness ($> 5 \cdot 10^6$ MPa) results in a constant velocity on the boundary nodes. Free boundary conditions are approximated with the use of very low ($< 5 \cdot 10^2$ MPa) stiffness values. Using intermediate stiffness values, the force applied on boundary nodes varies as a response to deformation processes within the model domain, except for rare instances in which a constant force is applied on boundary nodes that experience a very large mismatch between the plate motion and the boundary displacement. To best represent constant velocities far from the fault zone (i.e., at the boundaries of the very large models) the spring stiffness in the narrow-domain models was set to $5 \cdot 10^3$ to 10^4 MPa. This is similar to the value used in the models presented in this paper (10^4 MPa).

Appendix 3: Code Verification: Viscoelastic Component

To verify that the numerical procedure properly models viscoelastic deformation, we simulated postseismic surface deformation following a kinematically imposed earthquake, using a model in which no damage evolution was allowed. We compared our results with those from a viscoelastic finite-element model (GAEA, SAUCIER and HUMPHREYS, 1992). This extends previous comparisons which yielded interseismic velocities comparable to analytic solutions (LYAKHOVSKY *et al.*, 2001).

The two models were set up with identical domain size ($300 \times 250 \times 100$ km), fault depth (20 km), coseismic stress drop (20 MPa), lithospheric structure, and material properties ($\mu = 30$ GPa, $v = 0.25$, elastic plate thickness 20 km, and Newtonian substrate viscosity of 10^{19} Pa s). In both models the fault-parallel side and bottom boundaries were fixed, and the top boundary was stress-free. To simulate stress-free fault-perpendicular end boundaries our damage-disabled model incorporated the variable force boundary condition with a low stiffness, which is approximately equivalent to the stress-free boundary condition used in the FEM. Figure A2 shows surface velocities calculated with both models, for several time epochs after the modeled earthquake (1, 2, 5, and 18 years). The minor differences between the models are due in part to applying the variable force boundary condition with spring stiffness slightly too high (10^3 MPa) and therefore not simulating completely stress-free end boundaries. This slightly suppressed the velocities away from the fault.

REFERENCES

AGNON, A. and LYAKHOVSKY, V. *Damage distribution and localization during dyke intrusion*. In (G. Baer and A. Heimann, eds), *The Physics and Chemistry of Dykes* (Rotterdam, Balkema, 1995) pp. 65–78.

AMBRASEYS, N. N. (1970), *Some characteristic features of the North Anatolian fault zone*, Tectonophysics *9*, 143–165.

AMPUERO, J.-P. and BEN-ZION, Y. (2008), *Cracks, pulses and macroscopic asymmetry of dynamic rupture on a bimaterial interface with velocity-weakening friction*, Geophys. J. Int. *173*, 674–692, doi: 10.1111/j.1365-246X.2008.03736.x.

ANDREWS, D. J. (2005), *Rupture dynamics with energy loss outside the slip zone*, J. Geophys. Res. *110*, B01307, doi:10.1029/2004JB003191.

AYDIN, A. and JOHNSON, A.M. (1983), *Analysis of faulting in porous sandstones*, J. Struct. Geol. *5*, 19– 31.

ARMIJO, R., MEYER, B., KING, G. C. P., RIGO, A., and PAPANASTASSIOU, D. (1996), *Quaternary evolution of the Corinth Rift and its implications for the Late Cenozoic evolution of the Aegean*, Geophys. J. Int. *126*, 11–53.

BAISCH. S., and BOKELMANN, G. H. R. (2001), *Seismic waveform attributes before and after the Loma Prieta earthquake: Scattering change near the earthquake and temporal recovery*, J. Geophys. Res. *106*, 16,323-16,337.

BEN-ZION, Y. (1996), *Stress, slip and earthquakes in models of complex single-fault systems incorporating brittle and creep deformations*, J. Geophys. Res. *101*, 5677–5706.

BEN-ZION, Y. and AKI, K. (1990), *Seismic radiation from an SH line source in a laterally heterogeneous planar fault zone*, Bull. Seismol Soc. Am. *80*, 971–994.

BEN-ZION, Y. and ANDREWS, D. J. (1998), *Properties and implications of dynamic rupture along a material interface*, Bull. Seismol. Soc. Am. *88*(4), 1085–1094.

BEN-ZION, Y., HENYEY, T., LEARY, P. and LUND, S. (1990), *Observations and implications of water well and creepmeter anomalies in the Mojave segment of the San Andreas fault zone*, Bull. Seismol. Soc. Am. *80*, 1661–1676.

BEN-ZION, Y. and LYAKHOVSKY, V. (2006), *Analysis of aftershocks in a lithospheric model with seismogenic zone governed by damage rheology*, Geophys. J. Int. *165*, 197–210.

BEN-ZION, Y., PENG, Z., OKAYA, D., SEEBER, L., ARMBRUSTER, J. G., OZER, N., MICHAEL, A. J., BARIS, S. and AKTAR, M. (2003), *A shallow fault zone structure illuminated by trapped waves in the Karadere-Duzce branch of the North Anatolian Fault, western Turkey*, Geophys. J. Int. *152*, 699–717.

BEN-ZION, Y. and SAMMIS, C. (2003), *Characterization of Fault Zones*, Pure Appl. Geophys. *160*, 677–715.

BEN-ZION, Y. and SHI, Z. (2005), *Dynamic rupture on a material interface with spontaneous generation of plastic strain in the bulk*, Earth Planet. Sci. Lett. *236*, 486–496, doi: 10.1016/j.epsl.2005.03.025.

BERCOVICI, D. and RICARD, Y. (2003), *Energetics of a two-phase model of lithospheric damage, shear localization and plate-boundary formation*, Geophys. J. Int. *152* (3), 581–596 doi:10.1046/j.1365-246X.2003.01854.x

BUDIANSKY, B. and O'CONNELL, R. J. (1976), *Elastic moduli of a cracked solid*, Int. J. Sol. Struct. *12*, 81–97.

CARTER, N. L. and TSENN, M. C. (1987), *Flow properties of continental lithosphere*, Tectonophysics *136*, 27–63.

CHESTER, F. M. and CHESTER, J. S. (1998), *Ultracataclasite structure and friction processes of the Punchbowl Fault, San Andreas System, California*, Tectonophysics *295*, 199–221.

CHESTER, F. M. (1995), *Geologic studies of deeply exhumed faults of the San Andreas System, Southern California*: Collaborative research with Saint Louis University and Utah State University: NEHRP annual project summary, award No. 94G2457, v. 37.

CHESTER, F. M., EVANS, J. P., and BIEGEL, R. L. (1993), *Internal structure and weakening mechanisms of the San Andreas Fault*, J. Geophys. Res. *98*, 771–786.

CHRISTENSEN, N. I., and MOONEY, W. D. (1995), *Seismic velocity structure and composition of the continental crust: A global view*, J. Geophys. Res. *100* (B6), 9761–9788.

COCHRAN, E. S., VIDALE, J. E., and LI, Y. G. (2003), *Near-fault anisotropy following the Hector Mine earthquake*, J. Geophys. Res. *108*(B9), 2436, doi:10.1029/2002JB002352.

COWIE, P. A., VANNESTE, C., and SORNETTE, D. (1993), *Statistical Physics Model for the Spatiotemporal Evolution of Faults*, J. Geophys. Res. *98*(B12), 21,809–21,821.

CUNDALL, P. A. and BOARD, M. *A microcomputer program for modeling large-strain plasticity problems*. In *Numerical Methods in Geomechanics*, Proc. 6th Int. Conf. Numerical Methods in Geomechanics, Innsbruck, (ed. Swoboda), (C., Rotterdam, Balkema, 1988) pp. 2101–2108.

DE PAOLA, N., HOLDSWORTH, R. E., COLLETTINI, C., McCAFFREY, K. J. W., and BARCHI, M. R. (2007), *The structural evolution of dilational step-overs in regional transtensional zones*. (Cunningham W. D. and Mann,

P., eds), *Tectonics of Strike-Slip Restraining and Releasing Bends* (Geolog. Soc., London. Special Publications), *290*, pp. 433–445.

DIETERICH, J. H. (1972), *Time-dependent friction in rocks*, J. Geophys. Res. *77*, 3690–3697.

DIETERICH, J. H. (1978), *Time-dependent friction and the mechanics of stick-slip*, Pure Appl. Geophys. *116*, 790–805.

DIETERICH, J. H. (1979), *Modeling of rock friction 1. Experimental results and constitutive equations*, J. Geophys. Res. *84*, 2161–2168.

DOLAN, J. F., BOWMAN, D. D., and SAMMIS, C. G. (2007), *Long-range and long-term fault interactions in Southern California, Geology*, *35*, 855–858.

DOR, O., ROCKWELL, T. K. and BEN-ZION, Y. (2006), *Geological observations of damage asymmetry in the structure of the San Jacinto, San Andreas and Punchbowl Faults in Southern California: A possible indicator for preferred rupture propagation direction*, Pure Appl. Geophys. *163*, 301–349, doi:10.1007/s00024-005-0023-9.

DOR, O., YILDIRIM, C., ROCKWELL, T.K., BEN-ZION, Y., EMRE, O., SISK, M., DUMAN, T. Y. (2008), *Geologic and geomorphologic asymmetry across the rupture zones of the 1943 and 1944 earthquakes on the North Anatolian Fault: Possible signals for preferred earthquake propagation direction*, Geophys. J. Int., doi: 10.1111/j.1365-246X.2008.03709.x.

DUNHAM, E. M. and RICE, J. R. (2008), *Earthquake slip between dissimilar poroelastic materials*, J. Geophys. Res., in press.

EISSA, E. A. and KAZI, A. (1988), *Relation between static and dynamic Young's Moduli of Rocks*, Int. J. Rock Mech. Min. Sci. Geomech. Abstr. *25* (6), 479–482.

EVANS, J. P., SHIPTON, Z. K., PACHELL, M. A., LIM, S. J., and ROBESON, K. *The structure and composition of exhumed faults, and their implication for seismic processes*. In Proc. of the 3rd Confer. on *Tecto. problems of the San Andreas system*, (Stanford University 2000).

FIALKO, Y. (2004), *Probing the mechanical properties of seismically active crust with space geodesy: Study of the coseismic deformation due to the 1992 $M_w7.3$ Landers (southern California) earthquake*, J. Geophys Res. *109*, B03307, doi:10.1029/2003JB002756.

FIALKO, Y., SANDWELL, D., AGNEW, D., SIMONS, M., SHEARER, P., and MINSTER, B. (2002), *Deformation on nearby faults induced by the 1999 Hector Mine earthquake*, Science *297*, 1858–1862.

FINZI, Y., HEARN, E. H., LYAKHOVSKY, V., and BEN-ZION., Y. (2006), *3-D viscoelastic damage rheology models of strike-slip fault systems and their associated surface deformation*, EOS Trans. AGU, *87*(52), Fall Meet. Suppl., Abstract T21C-0425.

GRAYMER, R.W., LANGENHEIM, V.E., SIMPSON, R.W., JACHENS, R.C., and PONCE, D.A. (2007), *Relatively simple through-going fault planes at large-earthquake depth may be concealed by the surface complexity of strike-slip faults*. In (Cunningham, W.D., and Mann, Paul, eds.) *Tectonics of Strike-Slip Restraining and Releasing Bends*, (Geological Society of London Special Publication 2007), vol. 290, pp. 189–201, doi: 10.1144/SO290.5 0305-8719/07.

HAMIEL, Y., LYAKHOVSKY, V., and AGNON, A. (2005), *Rock dilation, nonlinear deformation, and pore pressure change under shear*, Earth Planet. Sci. Lett. *237*, 577–589.

HAMIEL, Y., KATZ, O., LYAKHOVSKY., RECHES, Z. and FIALKO, Y. (2006), *Stable and unstable damage evolution in rocks with implications to fracturing of granite*, Geophys. J. Int. *167*, 1005–1016.

HAMIEL, Y., LIU, Y., LYAKHOVSKY, V., BEN-ZION, Y., and LOCKNER, D. (2004), *A visco-elastic damage model with applications to stable and unstable fracturing*, Geophys. J. Int. *159*, 1155–1165.

HAMIEL, Y. and FIALKO, Y. (2007), *Structure and mechanical properties of faults in the North Anatolian Fault system from InSAR observations of coseismic deformation due to the 1999 Izmit (Turkey) earthquake*, J. Geophys Res. 112, B07412, doi:10.1029/2006JB004777.

HARRIS, R. A. and DAY, S. M. (1999), *Dynamic 3-D simulations of earthquakes on en echelon faults*, Geophys. Res. Lett. *26*, 2089–2092.

HARRIS, R. A. and DAY, S. M. (1993), *Dynamics of fault interaction: Parallel strike-slip faults*, J. Geophys. Res. *98*, 4461–4472.

HARRIS, R. A., ARCHULETA, R. J., and DAY, S. M. (1991), *Fault steps and the dynamic rupture process: 2-D numerical simulations of a spontaneously propagating shear fracture*, Geophys. Res. Lett. *18*, 893–896.

HEARN, E. H. and FIALKO, Y. (2009), *Coseismic deformation of Mojave compliant zones and crustal stresses*, J. Geophys. Res., in press.

HICKMAN, S., SIBSON, R.H., and BRUHN, R. (1995), *Introduction to a special section, mechanical involvement of fluids in faulting*, J. Geophys. Res. *100*, 12,831–12,840.

IDE, J. M. (1936), *Comparison of statically and dynamically determined Young's modulus of rocks*, Proc. Nat. Acad. Sci., U.S.A. *22*, 81–92.

KARABULUT, H. and BOUCHON, M. (2007), *Spatial variability and non-linearity of strong ground motion near a fault*, Geoph. J. Int. *170*, 1, 262–274.

KIM, Y. S., PEACOCK, D. C. P., and SANDERSON, D. J. (2004), *Fault damage zones*, J. Struct. Geology *26*, 503–517.

KING, G. (1986), *Speculations on the geometry of the initiation and termination processes of earthquake rupture and its relation to morphology and geological structure*, Pure Appl. Geophys. *124*, 567–585.

KIRBY, S. H. and KRONENBERG, A. K. (1987), *Rheology of the lithosphere: Selected topics*, Rev. Geophys. *25*, 1219–1244.

KORNEEV, V.A., NADEAU, R.M., and MCEVILLY, T.V. (2003), *Seismological studies at Parkfield IX: Fault-one imaging using guided wave attenuation*, Bull. Seismol. Soc. Am. *93*, 1415–1426.

LEWIS, M. A., PENG, Z., BEN-ZION, Y., and VERNON, F. (2005), *Shallow seismic trapping structure in the San Jacinto fault zone*, Geophys. J. Int. *162*, 867–881, doi:10.1111/j.1365-246X.2005.02684.x.

LI, Y. G., LEARY, P., AKI, K., and MALIN, P. (1990), *Seismic trapped modes in the Oroville and San Andreas fault zones*, Science, *249*, 763–766.

LI, Y.-G., AKI, K., ADAMS, D., HASEMI, A., and LEE, W. H. K. (1994), *Seismic guided waves trapped in the fault zone of the Landers, California, earthquake of 1992*, J. Geophys. Res. *99*(B6), 11,705–11,722.

LI, Y.-G., CHEN, P., COCHRAN, E. S., VIDALE, J. E., and BURDETTE, T. (2006), *Seismic evidence for rock damage and healing on the San Andreas fault associated with the 2004 M 6.0 Parkfield Earthquake*, Bull. Seismol. Soc. Am. *96*, 4B, S349–S363.

LIU, Y., TENG T. L., and BEN-ZION, Y. (2004), *Systematic analysis of shear-wave splitting in the aftershock region of the 1999 Chi-Chi earthquake: Evidence for shallow anisotropic structure and lack of systematic temporal variations*, Bull. Seismol. Soc. Am. *94*, 2330–2347.

LYAKHOVSKY, V. and MYASNIKOV, V. P. (1984), *On the behavior of elastic cracked solid*, Phys. Solid Earth *10*, 71–75.

LYAKHOVSKY, V. and MYASNIKOV, V. P. (1985), *On the behavior of visco-elastic cracked solid*, Phys. Solid Earth *4*, 28–35.

LYAKHOVSKY, V., BEN-ZION, Y., and AGNON, A. (1997a), *Distributed damage, faulting, and friction*, J. Geophys. Res. *102*, 27,635–27,649.

LYAKHOVSKY, V., RECHES, Z., WEINBERGER, R., and SCOTT, T.E. (1997b), *Non-linear elastic behavior of damaged rocks*, Geophys. J. Int. *130*, 157–166.

LYAKHOVSKY, V., BEN-ZION, Y., and AGNON, A. (2001), *Earthquake cycle, faults, and seismicity patterns in rheologically layered lithosphere*, J. Geophys. Res. *106*, 4103–4120.

LYAKHOVSKY, V., BEN-ZION, Y., and AGNON, A. (2005), *A viscoelastic damage rheology and rate- and state-dependent friction*, Geophys. J. Int. *161*, 179–190.

LYAKHOVSKY, V. and BEN-ZION, Y. (2008), *Scaling relations of earthquakes and aseismic deformation in a damage rheology model*, Geophys. J. Int. *172*, 651–662, doi: 10.1111/j.1365-246X.2007.03652.x.

LYAKHOVSKY, V., and BEN-ZION, Y. (2009), *Evolving fault zone structures in a damage rheology model*, Geochemistry, Geophysics, Geosystems, in review.

MALVERN, L.E. *Introduction to the Mechanics of a Continuum Medium* (New Jersey, Prentice-Hall, Inc., 1969), 713 pp.

MCGUIRE, J. and BEN-ZION, Y. (2005), *High-resolution imaging of the Bear Valley section of the San Andreas Fault at seismogenic depths with fault-zone head waves and relocated seismicity*, Geophys. J. Int. *163*, 152–164, doi: 10.1111/j.1365-246X.2005.02703.x.

MICKLETHWAITE, S. and COX, S. F. (2004), *Fault-segment rupture, aftershock-zone fluid flow and mineralization*, Geology *32*, 813–816.

MOONEY, W. D. and GINZBURG, A. (1986), *Seismic measurements of the internal properties of fault zones*, Pure Appl. Geophys. *124*, 141–157.

NADEAU, R., ANTOLIK, M., JOHNSON, P., FOXALL, W., and MCEVILLY, T. V. (1994), *Seismological studies at Parkfield III: Microearthquake clusters in the study of fault-zone dynamics*, Bull. Seismol. Soc. Am. *83*, 247–263.

OGLESBY, D. D., DAY, S. M., LI, Y.-G., and VIDALE, J. E. (2003), *The 1999 Hector Mine Earthquake: The dynamics of a branched fault system*, Bull. Seismol. Soc. Am. *93*, 6, 2459–2476.

OLSON, J., and POLLARD, D. D. (1989), *Inferring paleostresses from natural fracture patterns: A new method*, Geology *17*, 4, 345–348.

PENG, Z. and BEN-ZION, Y. (2004), *Systematic analysis of crustal anisotropy along the Karadere- Duzce branch of the north Anatolian fault*, Geophys. J. Int. *159*, 253-274, doi:10.1111/j.1365-46X.2004.02379.x.

PENG, Z. and BEN-ZION, Y. (2005), Spatio-temporal variations of crustal anisotropy from similar events in aftershocks of the 1999 M7.4 İzmit and M7.1 Düzce, Turkey, earthquake sequences, Geophys. J. Int. *160*(3), 1027–1043, doi: 10.1111/j.1365-246X.2005.02569.x.

PENG, Z. and BEN-ZION, Y. (2006), *Temporal changes of shallow seismic velocity around the Karadere-Duzce branch of the north Anatolian fault and strong ground motion*, Pure Appl. Geophys. *163*, 567–600, doi: 10.1007/s00024-005-0034-6.

PENG, Z., BEN-ZION, Y., MICHAEL, A. J., and ZHU, L. (2003), *Quantitative analysis of seismic trapped waves in the rupture zone of the 1992 Landers, California earthquake: Evidence for a shallow trapping structure*, Geophys. J. Int. *155*, 1021–1041.

POLIAKOV, A., CUNDALL, P., PODLADCHIKOV, Y., and LYAKHOVSKY, V. *An explicit inertial method for the simulation of viscoelastic flow: an evaluation of elastic effects on diapiric flow in two- and three-layers model*. In Proc. NATO Advanced Study Institute on *Dynamic Modeling and Flow in the Earth and Planets*, (Runcorn, K.E. and Stone, D., eds) (Dordrecht, Kluwer, 1993) pp. 175–195.

POUPINET, G., ELLSWORTH, W. L., and FRECHET, J. (1984), *Monitoring velocity variations in the crust using earthquake doublets: An application to the Calaveras Fault, California*, J. Geophys. Res. *89*(B7), 5719–5731.

POWELL, R. E. and WELDON, R. J. (1992), *Evolution of the San Andreas Fault*, Annu. Rev. Earth Planet. Sci. *20*, 431–468.

REVENAUGH, J. (2000), *The relation of crustal scattering to seismicity in southern California*, J. Geophys. Res. *105*(B11), 25,403–25,422.

RICE, J.R. and BEN-ZION, Y. (1996), *Slip complexity in earthquake fault models*, Proc. Natl. Acad. Sci. U.S.A. *93*, 3811–1818.

ROCKWELL, T. K. and BEN-ZION, Y. (2007), *High localization of primary slip zones in large earthquakes from paleoseismic trenches: Observations and implications for earthquake physics*, J. Geophys. Res. *112*, B10304, doi:10.1029/2006JB004764.

RUBINSTEIN, J.L. and BEROZA, G.C. (2004), *Evidence for widespread strong ground motion in the M_w 6.9 Loma Prieta eartquake*, Bull. Seismol. Soc. Am. *94*, 1595–1608.

RUDNICKI, J. W. and RICE, J. R. (2006), *Effective normal stress alteration due to pore pressure changes induced by dynamic slip propagation on a plane between dissimilar materials*, J. Geophys. Res. *111*, B10308, doi:10.1029/2006JB004396.

SAUCIER, F. and HUMPHREYS, E.D. (1993), *Horizontal crustal deformation in Southern California from joint models of geologic and very long baseline interferometry measurements*. In *Contributions of Space Geodesy to Geodynamics* (D.E. Smith and D.L. Turcotte, eds.), pp. 139–176, (AGU Geodyn. Ser. Vol. *23*, Washington D.C. 1993).

SCHAFF, D. P., BOKELMANN, G. H. R., BEROZA, G. C., WALDHAUSER, F., and ELLSWORTH, W. L. (2002), *High-resolution image of Calaveras Fault seismicity*, J. Geophys. Res. 107(B9), 2186, doi:10.1029/2001JB000633.

SCHAFF, D. P. and BEROZA, G. C. (2004), *Coseismic and postseismic velocity changes measured by repeating earthquakes*, J. Geophys. Res. *109*, B10302, doi:10.1029/2004JB003011.

SCHULZ, S. E. and EVANS, J. P. (2000), *Mesoscopic structure of the Punchbowl Fault, Southern California and the geologic and geophysical structure of active strike-slip faults*, J. of Struct. Geol. *22*, 913–930.

SEGALL, P. and POLLARD, D. D. (1980), *Mechanics of discontinuous faults*, J. Geophys. Res. *85*, 4337–4350, 1980.

SENGOR, A. M. C., TUYSZ, O., IMREN, C., SAKINC, M., EYIDOGAN, H., GORUR, N., LE PICHON, X., and RANGIN, C. (2005), *The North Anatolian Fault: A new look*, Annu. Rev. Earth Planet. Sci. *33*, 37–112.

SHELDON, H. A., and MICKLETHWAITE, S. (2007), *Damage and permeability around faults: Implications for mineralization*, Geology 35, 10, 903–906.

SHIPTON, Z. K., and COWIE, P. A. (2003), *A conceptual model for the origin of fault damage zone structures in high-porosity sandstone*, J. Struct. Geol. *25*, 3, 333–344

SIBSON, R.H. (1985), *Stopping of earthquake ruptures at dilational fault jogs*, Nature *316*, 248–251.

SIBSON, R. H. (2003), *Thickness of the seismic slip zone*, Bull. Seismol. Soc. Am. *93*, 3, 1169–1178.

STIRLING, M. W., WESNOUSKY, S. G., and SHIMAZAKI, K. (1996), *Fault trace complexity, cumulative slip, and the shape of the magnitude-frequency distribution for strikeslip faults: a global survey*, Geophys. J. Int. *124*, 833–868.

STIERMAN, D. J. (1984), *Geophysical and geological evidence for fracturing, water circulation and chemical alteration in granitic rocks adjacant to major strike-slip faults*, J. Geophys. Res. *89*, B7, 5849–5857.

SYLVESTER, A. G. (1988), *Strike-slip faults*, Geol. Soc. Am. *100*, 1666–1703.

SYLVESTER, A. G. and SMITH, R., (1976), *Tectonic transpretions and basement controlled deformation in the San Andreas fault zone, Salton trough, California*, AAPG Bull. *60*, 2081–2102.

TCHALENKO, J. S. (1970), *Similarities between shear zones of different magnitudes*, Geolog. Soc. Am. Bull. *81*, 1625–1640.

TEMPLETON, E. L. and RICE, J. R. (2008), *Off-fault plasticity and earthquake rupture dynamics, 1. Dry materials or neglect of fluid pressure changes*, J. Geophys. Res.

TENTHOREY, E., COX, S. F., and TODD, H. F. (2003), *Evolution of strength recovery and permeability during fluid-rock reaction in experimental fault zones*, Earth Planet. Sci. Lett. *206*(1–2), 161–172.

THURBER, C., ZHANG, H., WALDHAUSER, F., HARDEBECK, J., MICHAEL, A., and EBERHART-PHILLIPS, D. (2006), *Three-dimensional compressional wavespeed model, earthquake relocations, and focal mechanisms for the Parkfield, California, Region*, Bull. Seismol. Soc. of Am. *96*, 4B, S38–S49, doi: 10.1785/0120050825.

TURCOTTE, D. L. and GLASSCOE, M.T. (2004), *A damage model for the continuum rheology of the upper continental crust*, Tectonophysics *383*, 71–80.

WESNOUSKY, S. G. (2006), *Predicting the endpoints of earthquake ruptures*, Nature *444*, 358–360.

WESNOUSKY, S. (1994), *The Gutenberg-Richter or characteristic earthquake distribution, which is it*?, Bull. Seismol. Soc. Am. *84*, 1940–1959.

WILCOX, R. E., HARDING, T. P., and SEELY, D. R. (1973), *Basic wrench tectonics*, AAPG Bull. *57*, 74–96.

WU, C., PENG, Z. and BEN-ZION, Y. (2009), *Non-linearity and temporal changes of fault zone site response associated with strong ground motion*, Geophys. J. Int. *176*, 265–278, doi: 10.1111/j.1365-246x.2008.04005.x.

YAMASHITA, T. (2007), *Postseismic quasi-static fault slip due to pore pressure change on a bimaterial interface*, J. Geophys. Res. *112*, B05304, doi:10.1029/2006JB004667.

YANG, W. and BEN-ZION, Y. (2009), *Observational analysis of correlations between aftershock productivities and regional conditions in the context of a damage rheology model*, Geophys. J. Int., *177*, 481–499 doi: 10.1111/j.1365-246x.2009.0414s.

To access this journal online:
www.birkhauser.ch/pageoph